Loss of endogenous tau suppresses APOE4-induced patterned behavioral decline and axon dysmorphia in a *C. elegans* model of Alzheimer's disease

Eric A. Cardona[1], Chelsea J. Webber[1], Zheng Wu[1], Blythe M. Bolton[2], Elif Sarinay-Cenik[2], Jonathan T. Pierce[1]

[1]Department of Neuroscience, Center for Learning and Memory, University of Texas at Austin, Austin, TX

[2]Department of Molecular Biosciences, University of Texas at Austin, Austin, TX

* For correspondence: jonps@utexas.edu

ORCID for Eric A. Cardona: 0000-0001-8003-2691

ORCID for Chelsea J. Webber: 0000-0002-7715-2278

ORCID for Elif Sarinay-Cenik 0000-0001-8514-5505

ORCID for Jonathan T. Pierce: 0000-0002-9619-4713

Abstract

Alzheimer's disease (AD) causes a characteristic spatiotemporal pattern of neurodegeneration. The factors that account for this pattern of degeneration are unclear. Previously, we generated a model of AD using the nematode *Caenorhabditis elegans* with the AD risk variant of apolipoprotein E, *APOE4*. We showed that HSN class neurons degenerate in early adult animals. Here, we perform behavioral analyses to deduce the effect of APOE4 on the function of distinct neuronal circuits. We found evidence that APOE4 induces dysfunction of other neurons; this spatiotemporal pattern roughly correlates with endogenous levels of PTL-1, the *C. elegans* homolog of human MAPT also known as tau. Moreover, deletion of *ptl-1* suppressed defects in multiple behaviors, suggesting broad protective effects across the nervous system including the HSN neurons. Lastly, we show that PTL-1 in the touch receptor neurons, where PTL-1 is most abundant, contributes non-cell autonomously for age-related axon dysmorphia and dysfunction of the HSN neurons. Our results suggest that *C. elegans* may provide a useful

28 *in vivo* system to study how endogenous tau acts downstream of APOE4 to cause progressive,
29 patterned neurodegeneration.
30
31 **Introduction**
32 Neurodegenerative disorders such as Alzheimer's disease (AD), Parkinson's disease (PD), and
33 frontotemporal lobar dementia (FTLD) present with characteristic spatiotemporal patterns of
34 neuronal cell death (Braak and Braak, 1991; Bahia et al., 2013; Reviewed in Rietdijk et al.,
35 2017). Degeneration in characteristic brain regions corresponds to loss of brain region-
36 associated faculties, such as memory in AD (Rosen et al., 2005). Genetic risk factors have been
37 previously associated with AD. Among them, the ε4 variant of Apolipoprotein E (APOE4) is the
38 most common genetic risk factor for earlier onset and faster progression of sporadic AD and
39 AD-like pathology in individuals with Down syndrome (Larsen et al. 2024; Serrano-Pozo et al.,
40 2021). A recent study proposed that *APOE4* homozygosity itself may be a single-gene driver of
41 AD, akin to mutation of the familial AD genes *APP*, *PSEN1*, and *PSEN2* (Fortea et al., 2024;
42 Ryan and Rossor, 2010). Moreover, APOE4 has been shown to increase the severity of other
43 neurodegenerative diseases such as PD and FTLD (Robinson et al., 2018; Koriath et al., 2019;
44 Davis et al., 2020). How APOE4 worsens neurodegeneration (as in AD, PD, and FTLD) or,
45 more interestingly, may induce it (as suspected in AD) and contribute to patterned degeneration
46 is unclear.
47 As *APOE4* homozygosity alone may cause AD, it is critical to understand how APOE4
48 contributes to patterned neurodegeneration. One hypothesis is APOE4-induced
49 neurodegeneration follows a spatiotemporal pattern determined by cellular levels of specific
50 vulnerability factors. Multiple lines of evidence suggest that the microtubule associated protein
51 gene, *MAPT*, which encodes tau, represents one such vulnerability factor. First, pathogenic tau
52 forms intracellular aggregates, and their accumulation is closely linked to neuronal dysfunction
53 in AD and other degenerative disorders termed tauopathies (Trojanowski et al., 1993; Lin et al.,
54 2019). Second, tau-related pathology is highly correlated with neurodegeneration according to

55 Braak Staging, a well-established metric of how AD progresses with age (Braak and Braak,
56 1991; Köpke et al., 1993; Ghoshal et al., 2002). Third, transgenic expression of pathological tau
57 is sufficient to cause neurodegeneration (Mocanu et al., 2008; Spittaels et al., 1999;
58 www.alzforum.org/research-models). Fourth, depletion of endogenous tau mitigates cellular
59 correlates of AD pathology in rodent models of AD that overexpress human *APP* (Roberson et
60 al., 2007; Vossel et al., 2010) or human tau with aggregate-inducing mutations (Wegmann et al.,
61 2015; DeVos et al., 2017). Fifth, growing evidence suggests that pathogenic tau protein can
62 spread in a trans-synaptic fashion between brain regions *in vivo* with age (Liu et al., 2012; de
63 Calignon et al., 2012; Iba et al., 2013; Fu et al., 2016; Meisl et al., 2021; Cornblath et al., 2021).
64 Altogether, these and many other studies provide strong evidence for tau as a candidate
65 vulnerability factor underlying patterned neurodegeneration. Progress has been made to
66 uncover the relationship between APOE4, tau, and neurodegeneration (Shi et al., 2017;
67 Therriault et al., 2020; Seo et al., 2023; Koutsodendris et al., 2023), but whether APOE4 is a
68 causative factor in the pathogenic spread of tau or how APOE4 may contribute to a combination
69 of cell autonomous and non-cell autonomous processes is less clear. Additionally, because
70 rodent models of AD often do not fully recapitulate the neurodegeneration observed in human
71 patients, the cellular and molecular bases for this critical pathological phenotype have yet to be
72 uncovered.
73 The nematode *Caenorhabditis elegans* has been famously leveraged to discover
74 conserved *in vivo* mechanisms of cell death (Horvitz, 2003). It also represents a potentially
75 useful system to study the cellular and molecular bases for patterned neurodegeneration *in vivo*.
76 To model neurodegeneration, past studies have overexpressed human disease genes and
77 investigated the health and function of specific neurons *in vivo* (Faber et al., 1999; Baskoylu et
78 al., 2018; van Ham et al., 2008; Vaccaro et al., 2012b). In transgenic *C. elegans* models,
79 progress has been made to investigate genes involved with AD, notably *MAPT* and *APP*
80 (Kraemer et al., 2003; Treusch et al., 2011; Fatouros et al., 2012; Benbow et al., 2020; Sae-Lee
81 et al., 2020). A powerful feature of *C. elegans* as a model organism is that each one of its 302

82 neurons is identifiable. However, previous studies did not take full advantage of this to
83 investigate whether specific neurons differ in vulnerability due to tau. Thus, the potential of *C.*
84 *elegans* to test spatiotemporal patterns of neurodegeneration remains underutilized.
85 Here, we found that APOE4 induces a spatiotemporal pattern of behavioral decline in *C.*
86 *elegans* as inferred through the assessment of behaviors that reflect the activity of known
87 neurons. This pattern roughly correlates with neuronal expression levels of *ptl-1*, the sole worm
88 ortholog of *tau*. Complementing our indirect approach, we observed directly via live microscopy
89 that APOE4 induces progressive, age-related HSN axon dysmorphia coincident with dysfunction
90 of that neuron. Deletion of *ptl-1* suppressed both APOE4-induced behavioral defects and HSN
91 axon dysmorphia. Genetic ablation of the six neurons most enriched with PTL-1—the touch
92 receptor neurons (TRNs)—similarly suppressed HSN dysfunction; this was phenocopied by
93 targeted depletion of PTL-1 in the TRNs. These results suggest a non-cell autonomous role for
94 PTL-1 in APOE4-induced degeneration. Overall, our findings position the APOE4 worm model
95 as a useful system to study how endogenous tau/PTL-1 participates in the cellular and
96 molecular mechanisms underlying patterned neuronal dysmorphia or degeneration. This may
97 aid in the development of new therapeutic measures against tauopathies, such as AD.
98
99 **Results**
100
101 **APOE4 induces progressive, widespread behavioral defects in *C. elegans***
102 Our previous *C. elegans* study showed that pan-neuronal expression of APOE4 caused
103 degeneration and dysfunction in a subset of neurons—the HSN pair—in early adulthood, while
104 many others, such as VA and VB motor neurons, appeared healthy and functional (Sae-Lee et
105 al., 2020). In that work, we classified HSN neurons as degenerated when their somas appeared
106 shrunken or absent using a fluorescent reporter. Here, we extend this study by testing whether
107 APOE4 induces a broader pattern of neuronal dysfunction, neurodegeneration, or both. To do
108 this, we assayed multiple behaviors to probe the function of distinct neuronal subsets and

109 circuits, reasoning that behavioral performance would reveal the health of the underlying
110 neurons. We selected seven different behaviors that rely primarily, but not exclusively, on
111 mostly distinct subsets of identified neuron classes (Fig. S1). Five behaviors we tested—*egg*
112 *laying*, *pharyngeal pumping*, *gentle* and *harsh touch response*, and *locomotor gait transition*—
113 have specific neurons that are critical for behavioral execution. These include: the HSN class
114 neurons for egg laying behavior (Schafer, 2005); the MC and M3 neurons for pumping of the
115 pharyngeal feeding organ (Avery and You, 2012); the six TRNs for gentle touch response
116 (Chalfie and Sulston, 1981; Chalfie et al., 1985); the FLP and PVD neurons, with lesser
117 contribution from redundant mechanoreceptive neurons and interneurons, for harsh touch
118 response (Li et al., 2011); and lastly, the ADE and PDE dopaminergic neurons for the transition
119 between swim and crawl locomotor gaits (Vidal-Gadea et al., 2011). We also assessed two
120 readouts of locomotor behavior that rely on many more neurons with partial redundancy. *Short-*
121 *term locomotion* relies on over 100 motor neurons and about one dozen pre-motor interneurons;
122 *long-term locomotion* relies on those neurons and additional sensory neurons and interneurons
123 to mediate switches between roaming and dwelling states (Flavell, et al., 2020).
124 We evaluated behavioral performance at adult days 1 through 5 (D1-5) (Fig. 1A left).
125 This age range encompasses the peak reproductive period when *C. elegans* is active across a
126 range of behaviors and lays eggs (Scharf et al., 2021). We refer to “age of onset” of behavioral
127 decline as the first day of the adult stage that APOE4 worms displayed significantly impaired
128 behavior compared to age-matched controls.
129 Over the course of D1-5 of adult, we found that APOE4 worms displayed differences in
130 all seven behaviors compared to control (Fig. 1B-H). In as early as D1 adults, gentle touch
131 sensitivity, pharyngeal pumping, and short-term locomotion performances decreased by 11%,
132 13%, and 24%, respectively; gait transition decreased by a marked 59% (Fig. 1B-E). In D2
133 adults, long-term locomotion showed a 12% decline. We also replicated our previous finding of
134 an egg-laying defect that leads to larvae hatching internally, a salient phenotype called
135 “bagging” (Sae-Lee et al., 2020; Fig. 1G). APOE4 worms showed a salient 60% incidence of

136 bagging, peaking at D3. Whereas other behavioral performances declined, harsh touch
137 sensitivity oddly increased in APOE4 worms relative to control beginning at D3 (Figs. 1H, S2).
138 Altogether, these results indicate that APOE4 induces age-related abnormalities in multiple
139 behaviors that primarily rely on distinct subsets of neurons. Thus, the APOE4 worm exhibits a
140 wider spatiotemporal pattern of neuronal dysfunction, beyond the HSN neuron pair, across early
141 worm adult age.

142 The APOE4 worm exhibited a few defects in behaviors as early as D1 adults. To test
143 whether this represents a defect that originates during or after development we evaluated gentle
144 touch and pumping behaviors in L4 stage worms (~24 hours younger than D1 adults) out to D3
145 of adulthood for a new set of worms (Figs. 1A left, 2). A two-way ANOVA was used with planned
146 pairwise comparisons. Gentle touch and pumping behavior did not statistically differ between
147 control and APOE4 groups (compare L4 timepoints in Fig. 2A to 2B and 2C to 2D; see Fig. S3
148 with ages plotted together). Throughout adult stage, gentle touch remained unchanged as
149 expected into D1 and D3 for control (Pan et al., 2011), whereas sensitivity decreased in APOE4
150 ($p<0.02$). In contrast, while pumping rate in control worms increased as expected from L4 to D1
151 (Hosono et al., 1980; Huang et al., 2004; $p<0.05$ Fig. 2C), the rate remained unchanged in
152 APOE4 worms (Fig. 2D). Thus, there are likely to exist mixed or multiple mechanistic
153 underpinnings of APOE4-induced behavioral decline, such as age-related decline (as with
154 gentle touch) or developmental defects (as with pharyngeal pumping).
155

156 **APOE4-induced progressive behavioral defects depend on the worm ortholog of tau**

157 Above, we reported that gentle touch response is among the first behaviors to decline
158 with APOE4 on D1 adult. This behavior is mediated by the six TRNs that feature a prominent
159 array of microtubules that were exploited to discover the first microtubule gene (Chalfie and
160 Thomson, 1979; Chalfie and Thomson, 1982). Studies have shown that tau binds to and
161 stabilizes neuronal microtubules in mammals (Butner and Kirschner, 1991; Santarella et al.,
162 2004). As one may expect from microtubule-enriched neurons, the worm homolog of tau, PTL-1,

163 is highly enriched in the TRNs compared to other neurons, notably the PLM and ALM classes,
164 according to recent single-cell transcriptomic analyses (Taylor et al., 2021; Roux et al., 2023;
165 Fig. S4 green bars). We also noticed a rough correlation between endogenous levels of PTL-1
166 in specific neurons across the nervous system and the age of onset for APOE4-induced
167 behavioral decline. This is depicted in Fig. S1, where gray shows what fraction of *ptl-1* is
168 expressed in critical neurons that subserve each behavior. Given that tau represents a
169 pathological hallmark associated with neurodegeneration in AD, we speculated that the high
170 endogenous levels of PTL-1 in the TRNs may explain the early onset for the APOE4-induced
171 gentle touch defect. Following this idea, we also hypothesized that deletion of *ptl-1* may broadly
172 confer neuroprotection against APOE4. Into an APOE4 background we crossed a *ptl-1* mutant
173 bearing the *ok621* deletion allele (Δ*ptl-1*). This allele represents a strong hypomorph, if not a
174 null allele, as it lacks four exons that encode conserved microtubule-binding domains important
175 for PTL-1 function (Goedert et al., 1996; Gordon et al., 2008; Hashi et al., 2015; Figs. 1A right,
176 S5). Notably, the deleted region of PTL-1 contains residues conserved with mammalian tau that
177 promote aggregation when phosphorylated (Köpke et al., 1993).
178 We found that deletion of *ptl-1* significantly suppressed APOE4-induced defects in four
179 out of seven behaviors. Defects in gentle touch and pharyngeal pumping were completely
180 suppressed (Fig. 1B,C), while defects in gait transition and egg laying were partly suppressed
181 (Fig. 1D,G). We did not observe suppression of APOE4-induced abnormalities in short- and
182 long-term locomotion nor for harsh touch sensitivity (Fig. 1E,F,H). As a control, we found that
183 the *ptl-1* mutant was indistinguishable from control for six out of seven behaviors. Although the
184 *ptl-1* mutant displayed a moderate defect in swim-to-crawl transition compared to control, the
185 *ptl-1* mutant nonetheless partially suppressed the defect induced by APOE4 as opposed to
186 additively worsening the defect (Fig. 1D). Also, although *ptl-1* mutant displayed a non-significant
187 trend toward lower bagging compared to control animals, it significantly suppressed APOE4-
188 induced bagging (Fig. 1G).

189 Altogether, we conclude that PTL-1 variably contributes to the neuronal dysfunction
190 given multiple significant behavior changes induced by APOE4.
191
192 **APOE4-induced dysmorphia of HSN axon requires worm ortholog of tau**
193 Previously, we showed that APOE4-induced bagging coincided with what had appeared
194 to be degeneration of the bilaterally symmetric pair of HSN egg-laying motor neurons (Sae-Lee
195 et al., 2020). Because deletion of *ptl-1* suppressed APOE4-induced bagging, we hypothesized
196 that *ptl-1* deletion would also suppress HSN degeneration. To test this, we inspected the health
197 of reporter-labeled HSN neurons in live worms with epifluorescent microscopy. Dorsal to the
198 vulva, which is the egg-laying orifice, the HSNs are situated in the midbody of the worm
199 (depicted in Fig. 3A). To quantify degeneration, we initially calculated various metrics of HSN
200 soma geometry and reporter intensity across strains (Fig. S6A), focusing on D3 adult animals
201 which is the age of onset for increased bagging (~70% incidence in APOE4 worms; Figs. 1G,
202 3E).
203 Consistent with our previous study (Sae-Lee et al., 2020), we found that the HSN soma
204 appeared on average much dimmer in APOE4 than control worms, indicative of degeneration
205 (Fig. S6D). However, deletion of *ptl-1* alone also appeared to have caused dimming along with
206 abnormally large appearance of the HSN soma (Fig. S6B,D). We found no straightforward
207 relationship between other soma-based morphometrics and HSN dysfunction as reflected by
208 bagging incidence across control, *ptl-1*, and APOE4 strains (compare Fig. 1G to Fig. S6
209 measures). Thus, we conclude that HSN soma geometry and brightness are inconsistent
210 predictors of HSN function in these strains, possibly due in part to unforeseen aspects of the
211 fluorescent reporter (see Methods).
212 Seeking a more reliable cellular correlate of HSN function, we next investigated HSN
213 axon morphology. Previous work using laser ablation and mutants showed the proximal axon
214 portion (located between soma and vulval muscles)—but not distal portion which continues
215 anteriorly—is required for egg laying behavior (Garriga et al., 1993; Fig. 3A). Therefore, we

216 hypothesized that morphology of the proximal axon may serve as a useful correlate of HSN
217 neuron function.
218 We visualized the HSN proximal axon with the same fluorescent reporter as above for
219 the soma. The ~11 µm-long HSN proximal axon typically comprises two segments joined at a
220 right-angle (Fig. 3B image 1). The initial segment, which is qualitatively thicker, projects
221 anteriorly from the soma (segment i.) before turning ventrally at a right-angle into a second,
222 thinner segment (segment ii.) that joins the ventral nerve cord (VNC) and branches dorsally to
223 innervate egg-laying musculature. The unbranched, distal axon continues anteriorly within the
224 VNC to the head (Fig. 3A; Garriga et al., 1993). In our control reporter strain, we found that
225 ~58% of worms had a proximal axon with this typical two-segment, right-angle morphology
226 (N=93; Fig. 3B image 1), while the remainder had a single ventrally-projecting proximal axon
227 from the soma (Fig. 3B image 2). The latter single-segmented axons were thin and resembled
228 segment ii. of two-segment HSN proximal axons. We speculate that the thicker, anteriorly
229 directed segment i. did not develop in these worms because the HSN soma had already
230 migrated to a position directly dorsal from the vulval muscles. Although the HSN proximal axon
231 has been previously depicted with two segments connected at a right angle (Asakura et al.,
232 2007; Tsutsui et al., 2021), both configurations have been described in the literature and are
233 functional (Garriga et al., 1993). Thus, both types of proximal axons were scored as normal.
234 To check for axon abnormalities potentially caused by APOE4, we next qualitatively
235 scored the morphology of HSN proximal axons and quantified their lengths in D3 adult animals.
236 We found that the incidence of abnormal proximal axons was more than double in APOE4
237 compared to control worms. Proximal axons often took eccentric, elongated paths in APOE4
238 worms (compare Fig. 3B normal images 1,2 to abnormal images 3-10). This was not easily
239 explained by abnormal positioning of the HSN soma, as the somas were similarly located in
240 both APOE4 and control worms; soma positions were quantified as the HSN soma to VNC
241 distance and the HSN soma to vulva area distance (Fig. S7C left) or the angle formed between
242 these two vectors (Asakura et al., 2007; Fig. S7C right).

243 We observed at least three distinct qualitatively abnormal morphologies of the proximal
244 axons relative to control. First, segment i. (Fig. 3B, image 3) or segment ii. (Fig. 3B, image 4)
245 had an extra ~90-degree turn. Second, segment i. connected to segment ii. with a typical right-
246 angle turn, but displayed an atypical ~45-degree portion, with an apparently wider segment near
247 the soma (Fig. 3B images 5,6). Third, segments i. and ii. together took on a hook-like shape
248 oriented anteriorly (Fig. 3B images 7,8). We also noted additional cases (<5% frequency) where
249 these morphological abnormalities appeared to co-occur (e.g., segment ii. extra right-angle turn
250 and segment i. 45-degree portion, Fig. 3B, image 10). Overall, we conclude that APOE4
251 appears to induce a variety of proximal axon abnormalities of the HSN neurons.
252 To help distinguish whether the HSN proximal axon abnormality represented a
253 developmental defect, age-related degeneration, or both, we inspected younger adult animals to
254 determine when the defect started. In D1 adults, there was no significant difference in the
255 incidence of abnormal axons in APOE4 worms versus control (Fig. 3C). However, in D3 adults,
256 the incidence of abnormal axons showed a three-fold increase in APOE4 worms versus control
257 (Fig. 3D; see Fig. S8 with ages plotted together). Additionally, at the even younger L4
258 developmental stage, the entirety of HSN axon appears to project properly in ~95% of APOE4
259 animals (Fig. S9). From these observations, we deduce that the proximal axon defect begins by
260 at least D1 in some APOE4 worms and progresses in an age-related fashion, concurrent with
261 the age of onset for increased bagging and with similar incidence (Fig. 3G). We thus conclude
262 that the increased incidence in axon abnormality is likely to reflect a degenerative phenotype.
263 We next tested whether deletion of *ptl-1* might suppress APOE4-induced abnormal HSN
264 proximal axon morphology. To partly control for genetic background, we inspected two
265 independent isolates of APOE4;Δ*ptl-1* worms that were crossed with the HSN reporter strain.
266 For both isolates, we found that the *ptl-1* deletion suppressed the APOE4-induced abnormal
267 axon morphology (Fig. 3D).
268 The similar incidence of axon abnormality and bagging in APOE4 worms led us to
269 conclude that abnormal proximal axons reflect a defect in HSN function (compare control to

270 APOE4 in Figs. 1G, 3D,E). This is bolstered by our observation that deletion of *ptl-1* suppresses
271 APOE4-induced defects in behavioral performance as well as HSN proximal axon morphology.
272 Altogether, the above results support the idea that proximal HSN axon morphology is a reliably
273 predictive correlate of efficient egg-laying behavior and thus HSN health and function.
274 Although HSN axons were abnormally shaped in our study, we did not observe
275 consistent classical morphological signs of neuronal degeneration by D5 adulthood. Future
276 studies should determine whether such degenerative features emerge at later ages.

277 **Ablating tau-rich touch receptor neurons protects HSN from APOE4-induced dysfunction**

278 The spatiotemporal pattern of degeneration in AD is thought to be partly explained by
279 pathological forms of tau spreading between connected neurons and across the brain (intra-
280 and extra-synaptically; Liu et. al, 2012; de Calignon et al., 2012). As shown above, the systemic
281 deletion of *ptl-1* protected against age-related APOE4-incuded behavioral defects and abnormal
282 HSN proximal axon morphology. We next sought to test whether PTL-1 might contribute non-
283 cell autonomously to degeneration, explaining in part the spatiotemporal pattern of behavioral
284 decline in our APOE4 worm model. We hypothesized that targeting the neurons that are 1) most
285 abundant with PTL-1, and 2) tend to become dysfunctional early, may suppress the subsequent
286 degeneration of other neurons that express PTL-1 at a lower level. The TRNs represent the
287 neuronal class most abundant in PTL-1 in *C. elegans*. Over 30% of neuronal *ptl-1* transcripts
288 are expressed in the mere six TRNs (Taylor et al., 2021; Roux et al., 2023; Figs. S1,S4 green
289 bars). Coincidentally, the TRNs also become dysfunctional in D1 adults (Fig. 1B). In contrast,
290 the HSN neurons express ~80% less *ptl-1* than the TRNs and become dysfunctional later
291 starting in D3 adults (Figs. 1G,S3 blue bar; Taylor et al., 2021). Some TRNs are also nearby the
292 HSN neurons, such as the PLMs which synapse onto the HSN neurons (White et al., 1986).
293 Thus, the TRNs and HSN neurons in worm offer a convenient platform to test whether PTL-1
294 contributes non-cell autonomously to degeneration.
295 To assess the TRNs and PTL-1 protein *in vivo* during our targeted manipulations, we
296 took advantage of a control strain in which endogenous PTL-1 protein is translationally tagged

297 with mNeonGreen (PTL-1::mNG; Krieg, et al., 2017). Consistent with transcriptional studies
298 (Taylor et al., 2021), TRNs were readily visible in living larval and adult stages by their abundant
299 mNG-tagged PTL-1 (Representative PLM neuron in Figs. 4A2, 5B2). We also tested whether
300 the mNG tag on PTL-1 impedes its apparent neurotoxic properties downstream of APOE4. If
301 this were the case, we might expect less HSN dysfunction in APOE4;PTL-1::mNG worms.
302 Instead, we found bagging incidence in APOE4;PTL-1::mNG worms (60%) was similar to that of
303 the APOE4-alone strains generated in the current (~70%) and our previous (50-60%) studies
304 (note: all APOE4 strains depicted in Fig. 4A1 express mNG::PTL-1, versus those in Fig. 1G
305 which do not; Sae-Lee et al., 2020). We conclude that the endogenous mNG tag does not
306 interfere with the presumed toxicity of PTL-1 in an APOE4 background.
307 For our first targeted manipulation, we tested whether ablation of the TRNs suppresses
308 APOE4-induced HSN dysfunction. To do this, we leveraged the apoptotic trigger EGL-1, the
309 sole worm homolog of the human BH3-only domain proteins BAM and BID. Targeted
310 expression of *egl-1* has been previously used to kill specified cells (Chang et al., 2006). To kill
311 the TRNs, we generated a strain whose *egl-1* expression is driven by the promoter of *mec-17*, a
312 gene expressed exclusively in the TRNs (TRNs::EGL-1; Wu et al., 2025). The TRNs::EGL-1
313 strain was then crossed into the mNG-tagged *ptl-1* genetic background. To confirm the efficacy
314 of TRN genetic ablation, we first assayed gentle touch responses; we found that only 10% were
315 touch-responsive compared to control (N = 50). Second, we took advantage of the relative
316 abundance of mNG-tagged PTL-1 in the TRNs that could be directly observed using
317 epifluorescence microscopy (Fig. 4A2 control). Anatomically, this was easier to test with the
318 PLM class of TRNs due to how its soma and process are confined in the narrow tail region, in
319 contrast with the other TRN classes with soma situated in the thicker midbody (Fig. 4A2
320 control). We found that 93% of TRNs::EGL-1 animals had no detectable PTL-1::mNG where
321 PLM soma and processes were expected compared to control (N=46; Fig. 4A2). Third, we
322 confirmed ablation by imaging the PLM cell body with Differential Interference Contrast (DIC)
323 optics (Fig. S10). Together, these results suggest a successful cell ablation in most cases.

324 We found that ablating the TRNs partially suppressed APOE4-induced HSN dysfunction
325 as indicated by a ~30% reduction in bagging incidence (Fig. 4A1 yellow bar). Ablation of the
326 TRNs alone in the control strain had no effect on bagging (Fig. 4A1 white bar). Impressively,
327 ablating the TRNs conferred a similar magnitude of protection as afforded by systemic deletion
328 of *ptl-1* (compare blue bar in Fig. 1G to yellow bar in Fig. 4A1). Thus, we deduce that TRNs
329 activity and/or their cellular contents may contribute non-cell autonomously to APOE4-induced
330 HSN degeneration.
331 Because TRN activity is obviously lost after genetic ablation, we asked whether simply
332 blocking TRNs function alone as opposed to whole cell ablation may protect the HSNs against
333 APOE4. We tested this by using a deletion allele of *mec-4*, a gene that encodes
334 mechanoreceptive DEG/ENaC channel expressed predominantly in the TRNs (Chalfie and
335 Sulston, 1981). We took advantage of the *u253* loss-of-function allele of *mec-4*, referred hereon
336 as *mec-4*(*lf*), abolishes transduction of mechanosensory currents and gentle touch response yet
337 leaves the TRNs otherwise physiologically and morphologically normal (O'Hagan, et al., 2005).
338 We found that *mec-4*(*lf*) failed to suppress APOE4-induced HSN dysfunction (Fig. 4B). From
339 this, we conclude that functional impairment of the TRNs is insufficient to protect HSNs against
340 APOE4.
341 **Targeted reduction of tau in touch receptor neurons protects HSN against APOE4**
342 Because the worm ortholog of tau, PTL-1, is especially abundant in the TRNs (Fig. S4
343 green bars), we hypothesized that targeted depletion of PTL-1 contained in the TRNs would
344 protect against APOE4-induced HSN dysfunction, phenocopying TRNs ablation. To test this, we
345 knocked down *ptl-1* expression in the TRNs using cell-selective RNAi (TRNs::*ptl*-1 KD; Esposito
346 et al., 2007). To determine the efficacy and selectivity of the knockdown, we quantified PTL-
347 1::mNG fluorescence intensity in TRN soma versus example non-targeted neurons.
348 Conveniently, the soma of the non-targeted VC4 and VC5 class motor neurons are also easily
349 detectable by PTL-1::mNG fluorescence (Fig. 3A blue neurons; Fig. S4 blue bars). Compared to
350 control, TRNs::*ptl-1* KD worms had an average 40% decrease in PTL-1::mNG fluorescence in

351 five out of the six TRNs (Fig. 5A2). In contrast, PTL-1::mNG fluorescence intensity was
352 unchanged in the non-targeted VC4 and VC5 neurons (Fig. 5A2). These observations
353 suggested an effective and selective knockdown of *ptl-1* in the TRNs.
354 Using this strategy, we found that knockdown of *ptl-1* in the TRNs partially suppressed
355 APOE4-induced HSN dysfunction. This was determined after scoring bagging in two
356 independent isolates of APOE4 worms crossed with the TRNs::*ptl-1* KD strain to partly control
357 for genetic background (Fig. 5A1 blue bars). In contrast, knockdown of *ptl-1* in TRNs alone in
358 the control strain had no effect on bagging (Fig. 5A1 white bar). While significant, the
359 suppressive effect was noticeably weaker compared to the systemic *ptl-1* deletion (compare
360 with APOE4;Δ*ptl-1* strain, blue bar in Fig. 1G). We speculated that the weaker suppression may
361 be explained by RNAi reducing only a portion of *ptl-1* transcripts in the TRNs (Fig. 5A2). This
362 prompted us to test whether complete loss of *ptl-1* in the TRNs more strongly suppresses HSN
363 dysfunction than in APOE4;TRNs::*ptl-1* KD worms.
364 To achieve a targeted *ptl-1* knockout in the TRNs, we used an intersectional Cre-LoxP
365 approach. *LoxP* sites were first introduced via CRISPR to flank the endogenous *ptl-1*::*mNG*
366 locus (*LoxP*::*ptl-1*::*LoxP* strain). *LoxP*::*ptl-1*::*LoxP* worms were then crossed with a strain that
367 expresses Cre recombinase under the same TRNs-specific promoter as our TRNs::EGL-1 strain
368 (Harterink et al., 2018; Sanfeliu-Cerdán et al., 2023; Wu et al., 2025). This should result in a
369 selective knockout of *ptl-1* in the TRNs (TRNs::*ptl-1* KO). The efficacy of the *ptl-1* knockout was
370 confirmed first by evaluating the presence of PTL-1 in the PLM neurons via PTL-1::mNG
371 fluorescence signal (Fig. 5B2). PTL-1::mNG was absent in 100% of PLM neurons in TRNs::*ptl-1*
372 KO animals (N=45). Second, we confirmed the loss of the PLM cell body itself using Normarskii
373 optics (Fig. S10). Evaluation of protein by Western blot with the FLAG epitope on the tag using
374 whole-animal lysate was inconclusive due to high variability (Krieg et al., 2017; Fig. S11).
375 As with the knockdown, we found that knockout of *ptl-1* in the TRNs partially suppressed
376 APOE4-induced HSN dysfunction. This was determined after scoring bagging in two
377 independent isolates of APOE4 worms crossed with the TRNs::*ptl-1* KO strain to partially control

378 for genetic background (Fig. 5B1 blue bars). In contrast to the mild suppression after *ptl-1*
379 knockdown (Fig. 5A1 blue bars), the average extent of suppression by knockout in the TRNs
380 was more equivalent to that of the systemic deletion of *ptl-1* (Fig. 1G).

381 Finally, we inspected HSN axons directly to test whether knockout of *ptl-1* in the TRNs
382 suppresses APOE4-induced abnormal morphology. To do this, we generated new transgenic
383 reporter lines using our TRNs::*ptl-1* KO and APOE4;TRNs::*ptl-1* KO strains (Fig. 5B1 white and
384 left blue bar). In these strains, we observed no difference in the incidence of abnormal HSN
385 proximal axons comparing the no-APOE4 control to the APOE4 worms (Fig. 5B3). We conclude
386 that knockout of *ptl-1* in the TRNs is sufficient to suppress the axon morphology defects induced
387 by APOE4.

388 Does loss *ptl-1* in neurons other than the TRNs suppress APOE4-induced HSN
389 dysfunction? Aside from the TRNs, other sensory neurons in *C. elegans* are also abundant in
390 tau/PTL-1. These include a subset of over two dozen neurons that express the intraflagellar
391 transport protein CHE-2 in the ciliary basal body (Fujiwara et al., 1999; Taylor et al., 2021; Fig.
392 S4 yellow bars). As with our strategy for the TRNs, we generated a strain in which *ptl-1* was
393 knocked out in the these sensory neurons by crossing our *LoxP*::*ptl-1*::*LoxP* strain a strain
394 whose Cre recombinase expression is driven by the *che-2* promoter (CHEs::*ptl-1* KO). We
395 observed no significant suppression in APOE4;CHEs::*ptl-1* KO compared to APOE4 alone (Fig.
396 5C), suggesting PTL-1 in the broad set of *che-2*-expressing sensory neurons is not required for
397 APOE4-induced HSN dysfunction.

398 Altogether, we conclude that PTL-1 in the TRNs contributes non-cell autonomously to
399 APOE4-induced dysmorphia of the HSN neuron axons. We do not conclude that TRNs
400 represent the only source of harmful tau.

401

402 **Discussion**

403 **APOE4-induced pattern of behavioral decline in *C. elegans***

404 Here, we build on our prior work by characterizing APOE4-induced, age-related
405 abnormalities across seven behaviors in a *C. elegans* model of AD. The decline in behaviors
406 provides evidence for a spatiotemporal APOE4-induced pattern of neuronal dysfunction and
407 dysmorphia. Finally, we demonstrate that endogenous tau contributes to APOE4-induced axon
408 dysmorphia and multiple behavioral defects.
409 *C. elegans* has served as a leading model organism to study forms of cell death (Horvitz
410 2003). However, its potential to study mechanisms underlying *patterned neurodegeneration* in
411 response to human disease genes remains to be explored. This prompted us to ask whether
412 APOE4 worms display a pattern of neuronal dysfunction, dysmorphia or degeneration beyond
413 the HSN neurons as we previously reported (Sae-Lee et al., 2020). By day 4 (D4) of adulthood,
414 APOE4 worms exhibit defects of varying severity in all seven tested behaviors. Because each
415 behavior primarily relies on mostly distinct subsets of neurons (Fig. S1), this suggests a
416 progressive, neuron-specific pattern analogous to the characteristic progression observed in
417 human AD (Braak and Braak, 1991; Scahill et al., 2002; Fiford et al., 2018). The sensitivity of
418 certain behaviors to decline merits follow up studies to investigate putative higher-vulnerability
419 neurons (e.g., the ADE and PDE neurons required for swim-crawl gait transition; Vidal-Gadea et
420 al., 2011; Fig. 1D). Certain behaviors were not altered by pan-neuronal APOE4 expression,
421 perhaps indicating resilience to PTL-1-mediated degeneration or dysfunction. This idea is
422 mirrored in human AD where brain regions such as the somatosensory cortex and brainstem
423 are similarly spared from degeneration, even in advanced stages of AD (Rondina et al., 2018).
424 Alternatively, apparent resistance to APOE4 may reflect neuronal circuit redundancy. In this
425 vein, the subtle defects we observed in locomotion could reflect the functional redundancy of *C.*
426 *elegans* motor neurons (Izquierdo and Beer, 2018; Fig. 1E,F). Interestingly, harsh-touch
427 sensitivity subtly *increased* in APOE4 worms, hinting at neuronal hyperexcitability (Fig. 1H). In
428 mouse, APOE4-driven hyperexcitability may result from degeneration of inhibitory neurons
429 (Nuriel et al., 2017a). This aligns with fMRI studies of AD patients showing abnormally high
430 activity in certain brain regions (Bookheimer et al., 2000; Tuovinen et al., 2020). Future studies

431 could explore how APOE4 alters excitability of harsh touch neurons (e.g., the PVDs) and how
432 this may correlate with APOE4-induced progressive dysmorphia of the elaborate PVD dendrite
433 arborization (Jiang et al., 2025).

434 Axon dysmorphia, or axonopathy, is a hallmark of human AD characterized by neurite
435 deterioration and general white matter abnormalities (Lee et al., 2016). Similar axon defects,
436 sometimes without cell body loss, have been observed in human AD patients and mouse
437 neurodegenerative disease models (Leroy et al., 2007; Yoshiyama et al., 2007; Crespo-Biel et
438 al., 2014). Here, we identified APOE4-induced dysmorphia of the HSN proximal axon (Fig. 3).
439 Our findings suggest this reflects a degenerative phenotype rather than a developmental defect
440 because: HSN soma appear to migrate appropriately (Fig. S7), full axons project as expected in
441 pre-adult L4 stage animals (Fig. S9), and the incidence and timing of abnormal axon
442 morphology in D1 versus D3 adult APOE4 worms closely follow the HSN-associated egg laying
443 defect (Figs. 1G, 3E). Like neurons in mammals, worm neurons have been shown to contain
444 axonal domains with distinct structures and functions (Mizumoto and Shen, 2013; Eichel et al.,
445 2022). Future studies should consider what molecular factors might render the proximal HSN
446 axon vulnerable to dysmorphia. Overall, the tight correlation between a salient behavioral
447 phenotype (bagging; Fig. 1G, 3G) and axon dysmorphia of an identified neuron (HSN; Fig. 3)
448 provides a powerful system to study subcellular mechanisms of APOE4-induced axonopathy.
449

450 **Modeling degenerative mechanisms of tau in *C. elegans***

451 *C. elegans* has become increasingly recognized as a valuable *in vivo* model for studying
452 tau pathology (Reviewed in Natale et al., 2020). Along with extracellular amyloid-β plaques,
453 intracellular tau aggregation is a key pathological hallmark of AD (Kowall and Kosik, 1987; Kosik
454 et al., 1988; Grunke-Iqbal et al., 1986; Lee and Trojanowski, 1992). In AD and other
455 tauopathies, tau undergoes conformational changes that promote aggregation into tangles,
456 driving neurodegeneration (Friedhoff et al., 1998a,b; Jeganathan et al., 2006; Jeganathan et al.,
457 2008; Oakley et al., 2020). Unlike mammals, which have three broad tau-related gene families,

458 the worm has but a single endogenous homolog: *ptl-1* (Sündermann et al., 2016; Goedert et al.,
459 1996; Gordon et al., 2008). We found that deletion of *ptl-1* suppresses APOE4-induced defects
460 in four out of seven tested behaviors—including HSN-associated bagging—*and* HSN axon
461 morphological defects induced by APOE4. This parallels a previous report in a mouse AD model
462 in which APOE4-induced dysfunction of specific interneurons was suppressed by knocking out
463 endogenous murine tau (Andrews-Zwilling et al., 2010). Indeed, past immunohistochemical
464 evidence suggested that APOE and tau co-localize – and possibly physically interact – in
465 postmortem brain tissue from individuals with AD (Benzing and Mufson, 1995; Brecht et al.,
466 2004; Zhou et al., 2006; Rohn et al., 2012). Further studies showed that APOE4 expression
467 induces tau aggregates in cultured mouse neurons and worsens tau pathology in an AD mouse
468 model (Huang et al., 2001; Seo et al., 2023; Koutsodendris et al., 2023 Shi et al., 2017). It will
469 be interesting to see whether endogenous worm PTL-1 has similar pathological capacity
470 detectable at the biochemical level.

471 Depletion of endogenous tau was reported to protect against neurodegeneration in an
472 amyloid-β mouse model (Roberson et al., 2007). However, because *C. elegans* lacks an *APP*
473 ortholog whose protein product is capable of generating amyloid-β fragments (Daigle and Li,
474 1993), the benefits of PTL-1 reduction likely operate independently of amyloid-β. Interestingly, a
475 recent study found that *ptl-1* deletion partly mitigated age-dependent accumulation of
476 pathogenic human tau upon its overexpression in worm neurons (Nunez et al., 2022). Thus, the
477 APOE4 worm model of AD represents an Aβ-agnostic model to investigate how endogenous tau
478 contributes to patterned degeneration downstream of APOE4.

479 How might worm tau contribute to degeneration in our APOE4 worm model? PTL-1 may
480 contribute *cell-autonomously*. Notably, the pattern of behavioral decline roughly correlates with
481 endogenous *ptl-1* expression levels in the primary neurons underlying each behavior (Fig. S1).
482 This supports a model in which differences in baseline *ptl-1* expression set neuronal
483 vulnerability, with higher-expressing neurons reaching a pathological threshold earlier than
484 lower-expression neurons (Fig. S12). PTL-1 may also contribute *non-cell autonomously*. The

485 TRNs contain the majority of PTL-1 in the worm nervous system (Taylor et al., 2021; Roux et
486 al., 2023; Fig. S4 green bars). We found that depleting PTL-1 in the TRNs via genetic ablation,
487 RNAi-mediated knockdown, and Cre-LoxP-mediated knockout all partially suppressed APOE4-
488 induced dysfunction of HSN neurons. Each targeted manipulation roughly matched the
489 magnitude of suppression achieved by systemic *ptl-1* deletion. This raises the intriguing
490 possibility that, although *ptl-1* remains widely expressed, PTL-1 from the mere six TRNs is
491 required non-cell autonomously for HSN dysfunction.

492 Tau spread represents a popular non-cell autonomous hypothesis to explain the link
493 between tau pathology and spatiotemporal neurodegeneration in AD (Braak and Braak, 1991;
494 Reviewed in Braak and Del Tredici, 2011; Frost et al., 2010). Studies with tauopathy mouse
495 models have shown that pathological tau can propagate across synapses, starting from "seed"
496 regions rich in Tau (and high in inter-neuronal connectivity) and spreading to distant brain
497 regions (Clavaguera et al., 2009; Kfoury et al., 2012; Liu et al., 2012; de Calignon et al., 2012;
498 Iba et al., 2013). Similarly, we hypothesize that pathological PTL-1 may spread from neuron to
499 neuron over time in worm (Fig. S12). Although the six TRN soma are relatively distant from the
500 two HSN soma (1/2-1/3 body length or ~30-50 μm), PTL-1 is also enriched in TRN processes
501 which pass nearby the HSNs (Fig. 4A2). Two TRNs (the PLM pair) also form chemical synapses
502 with the HSNs (White et al., 1986). Future work could leverage synaptic transmission mutants to
503 test whether this represents a site of PTL-1 spread (Miller et al., 1996; McColluch et al., 2017). If
504 the hypothetical PTL-1 spread is synaptic, genetically perturbing TRN neurotransmission may
505 phenocopy our targeted manipulations described above, suppressing HSN dysfunction.
506 Because fluorescently tagged PTL-1 did not interfere with PTL-1-dependent degeneration of the
507 HSNs (compare APOE4 strains with mNG tagged PTL-1 in Figs. 4,5 to non-tagged PTL-1 in
508 Fig. 1G), our model may be used to directly visualize PTL-1 spread *in vivo*. With its simpler and
509 fully mapped nervous system, *C. elegans* offers a simple model to investigate how endogenous
510 tau propagates *in vivo* and contributes to APOE4-induced patterned neurodegeneration.

511 Deletion of worm tau did not equally protect against APOE4-induced behavioral
512 dysfunction. We found that deletion of *ptl-1* suppresses APOE4-induced defects in swim-to-
513 crawl switching and egg-laying ("bagging") more strongly than other behaviors (Fig. 1D,G).
514 Might inter-neuronal spread of tau explain this phenomenon? The synaptic connectivity of the
515 neurons underlying these behaviors offers a possible explanation (White et al., 1986). Swim-to-
516 crawl switching depends mainly on the dopaminergic neurons ADE and PDE, and egg-laying on
517 the HSN neurons (Trent et al., 1983; Vidal-Gadea et al., 2014). Notably, the PTL-1-rich TRNs
518 make direct chemical synapses onto these cells: AVM synapses onto ADE, and PLM synapses
519 onto PDE and HSN. In contrast, *ptl-1* deletion does not suppress APOE4-induced abnormalities
520 in short- or long-term locomotion or harsh-touch responses (Fig. 1E,F,H). Locomotion relies on
521 many motor neurons, and harsh touch depends on a redundant sensory circuit including PVD,
522 FLP, and touch neurons. Importantly, the TRNs do not directly synapse onto the DB and VB
523 motor neurons that drive forward locomotion, nor onto the PVD or FLP neurons involved in
524 harsh-touch sensing. Together, these connectivity patterns suggest a model in which PTL-1
525 produced in TRNs contributes to dysfunction in their postsynaptic partners (Fig. S12).
526 An alternate non-mutually exclusive hypothesis is that reduction of tau triggers
527 organism-wide or neuroprotective effects. The idea that tau levels set a susceptibility threshold
528 to many insults, not just tau-seeding pathology, may explain the broadly protective effects for
529 deleting tau in rodent models. For instance, Roberson et al. (2007) found that halving or deleting
530 endogenous tau rescued learning and memory as well as premature mortality in hAPP mice
531 without changing Aβ levels or plaques but also reduced susceptibility to chemically induced
532 seizures in otherwise wild-type backgrounds. Reducing tau also diminished spatial learning and
533 memory deficits after mild repetitive traumatic brain injury and attenuated axonopathy and other
534 histopathological changes in mice (Cheng et al, 2014). Systemic deletion of *ptl-1* reduces
535 lifespan in *C. elegans* (Chew et al., 2013; Chew et al., 2014) and was shown to be necessary
536 and sufficient in neurons for proper SKN-1-mediated response to environmental stressors
537 (Chew et al., 2015). It remains untested whether (and in what tissues) fine-tuning of PTL-1

538 levels may confer general protection against environmental and/or neurotoxic stressors in young
539 adult worms.
540 Regardless of how *ptl-1* contributes to degeneration, some APOE4-induced behavioral
541 defects persist even when *ptl-1* is deleted. Therefore, APOE4 must also impair neuronal
542 function through *ptl-1*–independent mechanisms. Future studies should investigate all the above
543 possibilities.
544

545 **Materials and Methods**

546 **Strain Maintenance**

547 Unless otherwise noted, worms were maintained at room temperature (~20 °C) on NGM plates
548 seeded with OP50 bacteria as described (Brenner et al. 1974). Strains with extrachromosomal
549 transgenes were propagated using selectable fluorescent reporters. Strains are listed in order of
550 appearance in figures:

551 **Figures 1 and S2**

JPS1451 *vxEx1211[Pmyo-3::mCherry::UNC54UTR]*

RB809 *ptl-1(ok621) III*

JPS1453 *vxEx1213[Prab-3::ND18ApoE4::UNC54UTR + Pmyo-3::mCherry::UNC54UTR]*

JPS1455 *vxEx1215[Prab-3::ND18ApoE4::UNC54UTR + Pmyo-3::mCherry::UNC54UTR]; ptl-1(ok621) III*

Figure 2

JPS1451 *vxEx1211[Pmyo-3::mCherry::UNC54UTR]*

JPS1453 *vxEx1213[Prab-3::ND18ApoE4::UNC54UTR + Pmyo-3::mCherry::UNC54UTR]*

Figures 3, S6, and S7

JPS1666 *vxIs591[ptph-1::GFP::unc-54UTR]; vxEx1211[Pmyo-3::mCherry::UNC54UTR]*

JPS1664 *vxIs591[ptph-1::GFP::unc-54UTR]; vxEx1211[Pmyo-3::mCherry::UNC54UTR]; ptl-1(ok621) III*

JPS1667 *vxIs591[ptph-1::GFP::unc-54UTR]; vxEx1213[Prab-3::ND18ApoE4::UNC54UTR + Pmyo-3::mCherry::UNC54UTR]*

JPS1778 *vxIs591[ptph-1::GFP::unc-54UTR]; vxEx1213[Prab-3::ND18ApoE4::UNC54UTR + Pmyo-3::mCherry::UNC54UTR]; ptl-1(ok621) III*

JPS1779 *vxIs59[ptph-1::GFP::unc-54UTR]; vxEx1213[Prab-3::ND18ApoE4::UNC54UTR + Pmyo-3::mCherry::UNC54UTR]; ptl-1(ok621) III*

Figure 4

JPS1571 *vxIs591[ptph-1::GFP::unc-54UTR]*

JPS1828 *vxEx1511[Pmec-17::EGL-1::egl-1UTR]*; *ptl-1(pg73[PTL-1::mNeonGreen])*

TU253 *mec-4(u253) X*

JPS1500 *vxIs824[prab-3::ND18ApoE4::UNC54UTR, pmyo-2::mCherry::UNC54UTR]; ptl-1(pg73[PTL-1::mNeonGreen])*

JPS1839 vx*Is824[prab-3::ND18ApoE4::UNC54UTR, pmyo-2::mCherry::UNC54UTR]; ptl-1(pg73[PTL-1::mNeonGreen]); vxEx1511[Pmec-17::EGL-1::egl-1UTR]*

JPS1709 *vxIs824[prab-3::ND18ApoE4::UNC54UTR, pmyo-2::mCherry::UNC54UTR]; ptl-1(pg73[PTL-1::mNeonGreen]); mec-4(u253) X*

Figure 5

JPS1571 *vxIs591[ptph-1::GFP::unc-54UTR]*

GN655 *ptl-1(pg73[PTL-1::mNeonGreen])*

JPS1456 *ptl-1(pg73[PTL-1::mNeonGreen]); vxEx1216[Pmec-17::ptl-1 sense and antisense CDS + Punc-122::RFP]*

JPS1819 *ptl-1(syb8686 syb8597 pg73[LoxP::PTL-1::mNeonGreen::LoxP) III; hrtSi99[Pmec-17::Cre]*

JPS1872 *ptl-1(syb8686 syb8597 pg73) III; mirIs42[Pche-2::Cre + Plin-44::GFP]*

JPS1500 *vxIs824[prab-3::ND18ApoE4::UNC54UTR, pmyo-2::mCherry::UNC54UTR]; ptl-1(pg73[PTL-1::mNeonGreen])*

JPS1581 *vxIs824[prab-3::ND18ApoE4::UNC54UTR, pmyo-2::mCherry::UNC54UTR]; ptl-1(pg73[PTL-1::mNeonGreen]); vxEx1216[Pmec-17::ptl-1 sense and antisense CDS + Punc-122::RFP]*

JPS1582 *vxIs824[prab-3::ND18ApoE4::UNC54UTR, pmyo-2::mCherry::UNC54UTR]; ptl-1(pg73[PTL-1::mNeonGreen]); vxEx1216[Pmec-17::ptl-1 sense and antisense CDS + Punc-122::RFP]*

JPS1823 *vxIs824[prab-3::ND18ApoE4::UNC54UTR, pmyo-2::mCherry::UNC54UTR]; ptl-1(syb8686 syb8597 pg73[LoxP::PTL-1::mNeonGreen::LoxP) III; hrtSi99[Pmec-17::Cre]*

JPS1824 *vxIs824[prab-3::ND18ApoE4::UNC54UTR, pmyo-2::mCherry::UNC54UTR]; ptl-1(syb8686 syb8597 pg73[LoxP::PTL-1::mNeonGreen::LoxP) III; hrtSi99[Pmec-17::Cre]*

JPS1898 *vxEx1604[pRAB-3::mCherry::unc-54utr]*; *ptl-1(syb8686 syb8597 pg73[LoxP::PTL-1::mNeonGreen::LoxP) III; hrtSi99[Pmec-17::Cre]*

JPS1899 *vxEx1605[pRAB-3::mCherry::unc-54utr + Prab-3::ND18ApoE4::UNC54UTR]*; *ptl-1(syb8686 syb8597 pg73[LoxP::PTL-1::mNeonGreen::LoxP) III; hrtSi99[Pmec-17::Cre]*

JPS1897 *vxIs824[prab-3::ND18ApoE4::UNC54UTR, pmyo-2::mCherry::UNC54UTR];ptl-1(syb8686 syb8597 pg73) III; mirIs42[Pche-2::Cre + Plin-44::GFP]/+*

Figure S8

GN655 *ptl-1(pg73[PTL-1::mNeonGreen])*

JPS1500 *vxIs824[prab-3::ND18ApoE4::UNC54UTR, pmyo-2::mCherry::UNC54UTR]; ptl-1(pg73[PTL-1::mNeonGreen])*

JPS1828 *vxEx1511[Pmec-17::EGL-1::egl-1UTR]*; *ptl-1(pg73[PTL-1::mNeonGreen])*

JPS1456 *ptl-1(pg73[PTL-1::mNeonGreen]); vxEx1216[Pmec-17::ptl-1 sense and antisense CDS + Punc-122::RFP]*

JPS1819 *ptl-1(syb8686 syb8597 pg73[LoxP::PTL-1::mNeonGreen::LoxP) III; hrtSi99[Pmec-17::Cre]*

552 **Generation of strains**

553 The 1933 bp deletion in *ptl-1* allele *ok621* was confirmed by PCR using the following primers
554 (written in 5'-3' orientation):

Forward: CTGGAAATTTGTTGGGCAGT

Reverse: TGAACCGAAGCCTAAACCAG

555 We sought to independently confirm the effect of pan-neuronal APOE4 on egg laying as well as
556 to test other behaviors with new extrachromosomal transgenic strains that carry a new reporter
557 that minimized effects on multiple behaviors. We transformed wild-type N2 with 20 ng/μL of the
558 APOE4 plasmid pPS90 (Sae-Lee et al., 2020) along with 10 ng/μL of the pCFJ104 mCherry
559 body wall reporter (Frøkjaer-Jensen et al., 2008) to generate the new extrachromosomal strain
560 JPS1453. In parallel, we transformed the *ptl-1*(*ok621*) mutant strain RB809 with the same DNA
561 mixture yielding the APOE4;Δ*ptl-1* strain JPS1455. We also generated control strain JPS1451
562 that carries the mCherry reporter alone.

563 To visualize HSN axons, we first used the GFP reporter strain JPS1571. This strain was
564 crossed with JPS1451 and JPS1453 to yield the control and APOE4 strains JPS1666 and
565 JPS1667, respectively. JPS1666 was then crossed with RB809 to yield the *Ptph-1::gfp*;Δ*ptl-1*
566 strain JPS1664. JPS1667 was crossed with RB809 to yield APOE4;Δ*ptl-1*, from which two
567 independent isolates were obtained, JPS1778 and JPS1779, to partly control for genetic
568 background (Fig. 3). In our independent reporter lines, we transformed strain JPS1819 with 20
569 ng/uL of the mCherry reporter plasmid pGH8 without or with 40 ng/uL APOE4 plasmid pPS90 to
570 yield strains JPS1898 and JPS1899 (Fig. 5B3).

571 **Cell-specific gene knockdown**

572 To knock down *ptl-1* specifically in the TRNs, we followed previous methods by Esposito et al.
573 (See Fig. 1 of Esposito et al., 2007). The *mec-17* promoter (1535 bp) was fused with either
574 sense or antisense of *ptl-1* coding region (820 bp) to generate separate DNA fragments using
575 the following primers (written in 5'-3' orientation):

A

Forward: GGCTTGAATAATCCCTATTATAGCC

Reverse: GAAATTACCTGAAATTTCGTGGGG

B

Forward: GAGAAAACGGCCAATTGACGC

Reverse: GGCTATAATAGGGATTATTCAAGCCGATCGAATCGTCTCACAACTG

C

Forward: GAGAAAACGGCCAATTGACGC

Reverse: CCCCACGAAATTTCAGGTAATTTCGATCGAATCGTCTCACAACTG

D

Forward: CGTCGCGCTAACAGTTCTAG

Reverse: CCAAAGGTTAACGCCAAATTTG

E

Forward: CGTCGCGCTAACAGTTCTAG

Reverse: CAAGTGAAAGCGTGGTCCGATC

576 Fragments D and E were mixed in equimolar amounts, along with a selectable RFP
577 coelomocyte marker (Addgene Plasmid #8938), to a final concentration of 80 ng/µL. This DNA
578 mix was transformed into the *ptl-1*::*mNeonGreen* strain GN655 (PTL-1::mNG; Krieg et al.,
579 2017). The resultant strain, JPS1456, expresses *ptl-1* dsRNA fragments in the TRNs. JPS1456
580 was crossed into JPS1500, which carries an integrated pan-neuronal APOE4 transgene; this
581 yielded APOE4;TRNs::*ptl-1* KD from which two independent isolates were obtained, JPS1581
582 and JPS1582, to partly control for genetic background.

583 **Cell-specific gene knockout**

584 To knock out *ptl-1* in the TRNs, we commissioned SUNY Biotech to generate the strain
585 PHX8686 which harbors *LoxP* sites flanking the *ptl-1* genetic locus in the strain GN655.
586 PHX8686 was crossed into MSB1167, a transgenic line in which Cre recombinase is expressed
587 under control of the *mec-17* promoter (Harterink et al., 2018). This yielded the TRNs::*ptl-1* KO
588 strain JPS1819. The presence of PTL-1::mNG in the TRNs was determined with epifluorescent
589 microscopy. Lastly, JPS1819 was crossed into JPS1500 to yield APOE4;TRNs::*ptl-1* KO, from

590 which two independent isolates were obtained, JPS1823 and JPS1824, to partly control for
591 genetic background.
592 Similarly, knockout of *ptl-1* in the *che-2*-expressing subset of sensory neurons (CHEs)
593 was achieved by crossing PHX8686 into FX16644, a transgenic line in which Cre recombinase
594 is expressed under control of the *che-2* promoter (National BioResource Project, Japan). This
595 yielded the CHEs::*ptl-1* KO strain JPS1872. However, subsequent crossing into JPS1500
596 resulted in synthetic lethality in animals homozygous for the CHEs-specific Cre transgene.
597 Thus, heterozygotes were selected for egg laying behavior assays.
598 **Cell-specific ablation**
599 To genetically ablate the TRNs, we used the TRN-specific *mec-17* promoter to express *egl-1* in
600 an extrachromosomal array in strain JPS1828 (Wu et al., 2025). This strain was crossed into
601 JPS1500, a strain carrying an integrated pan-neuronal APOE4 transgene and a *Punc-122*::*gfp*
602 reporter, to yield strain JPS1839. Additionally, we crossed JPS1500 into TU253, which carries a
603 *mec-4* loss-of-function mutation (O'Hagan et al., 2004), to yield the APOE4;*mec-4*(*lf*) strain
604 JPS1709.
605 **Sterilization**
606 To inspect HSN neuron health without confounding effects of the bagging phenotype, worms
607 were sterilized as previously described (Mitchell et al., 1979). In brief, seeded plates were
608 pretreated with 600 mL of 0.8 mM 5'-fluorodeoxyuridine (FUdR; FUdR plates). Mid- to late-stage
609 L4 stage worms were transferred onto FUDR plates and moved to fresh FUdR plates every 1-2
610 days as needed.
611 **Behavioral assays**
612 Behavioral assays were performed on either 60 mm (medium) or 35 mm (small) NGM plates,
613 seeded or not with OP50 bacteria as described per assay. All assays were performed at room
614 temperature (20° C) unless stated otherwise. Assays began with day 1 adults (D1), 24 hours
615 after initial incubation on FUDR plates (if applicable), until a significant difference between

616 control and APOE4 worms was observed. Completely immobile worms or those which escaped
617 from the side of the plate were omitted from assays and final quantifications.

618 **Gentle touch**

619 Methods adapted from Chalfie and Sulston (1981). In brief, 20-30 worms were moved to
620 medium NGM-OP50 plates. To test gentle touch sensitivity, an eyelash hair, affixed by its shaft
621 to a pipette tip, was used to deliver mechanical stimuli to worms. Gentle strokes were applied to
622 the posterior and anterior of the animal. Six paired anterior and posterior stimuli were applied,
623 with an interstimulus interval of approximately 1.5 seconds to avoid habituation. Gentle touch
624 sensitivity was quantified per worm as the fraction of responses to stimuli out of 12.

625 **Harsh touch**

626 Methods adapted from Li et al. (2011). In brief, 20-30 worms were moved to medium NGM-
627 OP50 plates. To test harsh gentle touch sensitivity, a single prod was delivered to the mid-body
628 using a platinum pick. Five technical replicates were performed per worm per strain. Harsh
629 touch sensitivity was quantified per replicate as the proportion of responsive worms.

630 **Pharyngeal pumping**

631 Methods adapted from Avery and Shtonda (2003). In brief, 30-40 worms were first moved to
632 medium NGM-OP50 plates. Worms were allowed to roam for at least 30 minutes. Individual
633 animals were then tracked for 20 seconds and pharyngeal bulb contractions were manually
634 tallied with a handheld click counter. Pumping rate was quantified per worm as pumps per
635 minute.

636 **Bagging**

637 Methods adapted from Sae-Lee et al. (2020). In brief, at least 30-40 L4-stage worms were
638 moved to medium NGM-OP50 plates. Worms were scored daily for the internal hatching or
639 “bagging” phenotype based on presence or absence of several late-stage eggs and/or hatched
640 larvae within the uterus; this is often accompanied by general lethargy plus distension of the
641 worm midbody as previously described (Trent et al., 1983). Bagging worms were tallied and
642 discarded while non-bagging worms were transferred to a fresh medium NGM-OP50 plate.

643 Worms were scored in this fashion from D1 to D4 of adulthood. Bagging incidence was
644 quantified per replicate as the cumulative percentage of bagging worms summed across D1-4
645 out of the original total.

646 **Long-term locomotion**

647 Methods adapted from Nordquist et al. (2018). Single worms were moved to the center of a
648 small NGM plate uniformly seeded with OP50 such that the lawn covered the entirety of the
649 NGM surface. Animals were incubated on these assay plates overnight at 22°C. Groups of at
650 least 8 worms per genotype were tested on two separate days as also described by Nordquist
651 et al. After 18 hours, the worms were removed from their plates and a transparent grid guide
652 was used to determine the number of ~5 mm^2 regions (32 in total) traversed on the assay plate.
653 Regions encompassing parts of the agar that split or pulled away from the plastic of the plate
654 were omitted from the total. Long-term locomotion was quantified per worm as the proportion of
655 traversed regions on the assay plate out of the total.

656 **Short-term locomotion**

657 Methods adapted from Topalidou et al. (2017). In brief, 8-10 worms were moved to the center of
658 a medium NGM-OP50 plate that was uniformly seeded such that the bacterial lawn extended
659 across the entire medium surface. After 10 minutes, worms were removed and their final
660 positions marked on the plate. Groups of least 15 worms per genotype were tested on two
661 separate days as previously described (Nordquist et al., 2018). Radially dispersed distance was
662 recorded. Short-term locomotion was quantified per worm as the distance (cm) from the center
663 to final positions.

664 **Swim-to-crawl gait transition**

665 Methods adapted from Vidal-Gadea et al. (2011). Before testing, 25-40 worms were moved to a
666 medium NGM plate and allowed to roam for ~15 minutes so excess OP50 could be removed.
667 Meanwhile, assay plates were prepared by first drawing a 0.5 cm radius border on the plastic
668 behind its center. Next, 10 uL of liquid NGM was pipetted to the very center of the assay plate
669 surface. Worms were then picked to the center of the puddle on the assay plate and a 15-

670 minute timer was started. As the puddle dried, swimming worms began to escape to the solid
671 surface, transition to a crawling gait, and disperse away from the puddle. Gait transition was
672 quantified per replicate as the proportion of worms that escaped and crawled past the 0.5 cm
673 border in under 15 minutes.

674 **Microscopy**

675 Epifluorescent microscopy was performed on an Olympus IX51 inverted microscope with an
676 Olympus UPlanFL N 40X/0.75 NA objective and X-Cite FIRE LED Illuminator (Excelitas
677 Technologies Corp.). Images were captured using a Retiga 2000R CCD camera (QImaging)
678 and QCapture Pro 6.0 software.

679 Worms were sterilized with FUDR as described above to prevent internally hatching
680 larvae that may affect HSN morphology. Worms were then mounted on 2% agarose pads and
681 immobilized using 50 mM sodium azide. All imaging per pad took place within 30 minutes of
682 mounting.

683 The same fluorescence intensity settings were used to image all HSN soma and
684 proximal axons via a GFP reporter. Importantly, imaging was restricted to worms that lay in a
685 strictly lateral orientation (i.e., on the right or left side with minimal twisting about the long axis of
686 the animal). This ensured both the soma and proximal axon of a given HSN neuron were in
687 approximately the same focal plane. We determined the orientation of mounted worms using the
688 fluorescent co-injection marker. This marker labels body wall and vulval musculature with
689 mCherry, visualizable in the red channel. In single focal planes, the labeled vulval muscles
690 either appear as an x-shape from a ventral viewpoint or a v-shape if the animal laid directly on
691 its right or left side as described above (See also Fig. 1 of Collins and Koelle, 2020).
692 Incidentally, the HSN GFP reporter also labels the VC4 and VC5 motor neurons which are
693 visible in the same focal plane. These guides helped restrict our microscopy to animals in the
694 desired orientation described above.

695 After imaging, morphometrics of HSN soma and proximal axons were calculated in
696 ImageJ (Schneider et al., 2012). Positions of HSN soma were determined by measuring the

697 lengths of the vector from the soma to the ventral nerve cord (HSN-VNC, met at a
698 perpendicular) and the vector to the vulval area in between VCs4,5 (HSN-vulva). These
699 measurements were also collapsed into a single metric as previously described (Asakura et al.,
700 2007). This metric, represented by θ, is the angle in degrees between the HSN-vulva
701 (hypotenuse) and HSN-VNC (adjacent) vectors (i.e., arccosine of their ratio).

702 HSN proximal axon lengths were calculated with the NeuronJ plugin for ImageJ using
703 default settings (Meijering et al., 2004). Traces were made by following the proximal axon from
704 anterior face of the HSN soma to the point at which the axon exits the focal plane ventrally in
705 the vulval area. Ectopic sprouts from the soma or proximal axon were excluded from tracing. In
706 the rare (<5% frequency) cases where ectopic sprouts were present on the proximal axon, the
707 shortest ventral- and vulval-directed course was traced for all strains imaged.

708 Full HSN axons were imaged in mid- to late-L4 stage worms when full projection to the
709 head region is typically complete (Garriga et al., 1993). Worms with very dim GFP fluorescence
710 were excluded from scoring, as it was ambiguous whether axons failed to project or the reporter
711 transgene was not yet highly enough expressed.

712 To capture images of PTL-1::mNG strains, an increased exposure time and intensity
713 setting were required compared to HSN GFP reporter strains. Because some TRN processes
714 span nearly the entire animal length, we chose to focus on soma to quantify PTL-1::mNG signal
715 in TRNs::*ptl-1* KD strain JPS1456 and control strain GN655 (See Fig. 4). Depending on animal
716 orientation, bilateral TRN soma were identifiable based on the naturally asymmetric positioning
717 of the AVM and PVM class neurons (Arnold et al., 2020). The VCs4,5 neurons were almost
718 always visualizable regardless of orientation, making them ideal for internal controls.
719 Fluorescence intensity was quantified in ImageJ in day 1 adults.

720 In the TRNs::*ptl-1* KO strain JPS1819, *LoxP*-flanked *ptl-1* is presumably excised by Cre
721 recombinase whose expression is driven by the *mec-17* promoter (Harterink et al., 2018).
722 Although *mec-17* expression begins embryonically in ALM and PLM class TRNs (Roux et al.,
723 2023), residual PTL-1::mNG is still present by at least L4 stage of development; PTL-1::mNG is

724 qualitatively fainter in those cells compared to like-aged control animals (GN655 strain). Thus,
725 selection for animals with lacking PTL-1::mNG in PLM neurons was conducted in at least day 1
726 adults to avoid ambiguity. This selection strategy was also employed in the TRNs::EGL-1 strain
727 JPS1828 to identify animals with genetically ablated TRNs.

728 **Western blotting**

729 Worms were washed twice with 5% sucrose and twice with 50 mM NaCl before being
730 flash frozen with 5µl glass beads. For worm lysis, 2% PMSF was added to 2x Laemmli buffer.
731 This buffer was then addedto the frozen samples to achieve a 1x concentration. Finally, 5% β-
732 mercaptoethanol (BME) was added to the samples, followed by bead beating for 30 seconds.
733 Samples were spun down through centrifugation for 2 minutes at 15,000 g. The samples were
734 then boiled a t 95℃ for 5 minutes. An additional 2-minute centrifugation was performed to clear
735 debris prior to measuring protein concentration with Qubit Protein Assay Kit (Thermo Scientific,
736 #Q33211).

737 20 µg of protein per sample was loaded on Invitrogen™ NuPAGE™ Bis-Tris Mini
738 Protein Gels (4–12%, 1.0–1.5 mm, Invitrogen, #NP0335) and separated at 80-120 V in
739 1X MES SDS running buffer. Proteins were transferred onto a PVDF membrane
740 (Thermo Scientific, #88518) at 30V for 1 hour.

741 Membranes were blocked in 1X TBS Tween 20 Buffer (Thermo Scientific, #28360)
742 containing 5% milk. Flag tag and actin were probed with primary antibodies: Monoclonal
743 ANTI-FLAG® M2 antibody produced in mouse (1:2,000, Sigma-Aldrich, #F3165) and
744 Anti-Actin Mouse Monoclonal Antibody [clone: C4] (1:500, MP Biomedicals,
745 #08691001), respectively. A secondary antibody, Goat anti-Mouse IgG (H+L)
746 Superclonal™ Secondary Antibody, Alexa Fluor™ 488 (1:4,000, Invitrogen, #A28175)
747 was used after flag and actin probing. Finally, an Amersham™ Typhoon™ RGB was
748 utilized for visualization.

749 **Statistical analysis**

750 All data are presented as the mean ± SEM. Plotted data points represent individuals or the
751 average across a single replicate as indicated in figures. Total sample size (N) is indicated in
752 figure legends. Behavioral assays and microscopy scoring were performed blind to genotype.
753 Planned χ^2 tests of independence were performed for statistical comparisons of gait transition
754 (escaped vs. not escaped), bagging (yes vs. no), and HSN axon scoring (normal vs. abnormal)
755 in Excel 2022 (365 MSO, Version 2510 Build 16.0.19328.20190, 64-bit). Touch, pumping, and
756 locomotion behaviors, HSN axon length, HSN soma position, and fluorescence intensity were
757 compared with planned, Student t-tests or post hoc comparisons following two-way ANOVA
758 tests (SPSS, v29.0.2.0, IBM).
759

760 **Acknowledgements**

761 We would like to thank Drs. Miriam B. Goodman and Michael Krieg for sharing strains GN655
762 and MSB1167, respectively, and SUNY Biotech for engineering PHX8686. Some strains were
763 also provided by the *Caenorhabditis* Genetics Center, which is funded by the NIH (P40
764 OD010440),. We also thank Dr. Lotti Brose and Anna Krauss for preliminary experiments with
765 APOE4; Δ*ptl-1* animals.

766

767 **Footnotes**

768 **Author contributions**

769 Conceptualization: J.T.P., E.A.C.; Methodology: E.A.C., Z.W., J.T.P.; Investigation: E.A.C.,
770 Z.W., B.M.B., C.J.W., E.S.-C., J.T.P.; Writing – original draft: E.A.C., J.T.P.; Writing – review
771 and editing: E.A.C., Z.W., C.J.W., E.S.-C., J.T.P.; Funding acquisition: E.S.-C., J.T.P.

772 **Funding**

773 This work was funded in part by the NIH (R01GM122463, RF1AG057355, R21OD032463 -
774 J.T.P.) Waggoner Fellowship for Alcohol Research (J.T.P.), David and Ellen Berman
775 Fellowships for Huntington's Research (J.T.P.), George and Karen Casey (J.T.P.), Pine Family
776 Foundation (J.T.P.), CNS Catalyst Grant (J.T.P. and E.S.C.), National Institutes of Health (NIH)
777 NIGMS (R35GM138340) (E.S.C.), NIH T32 MH106454 (C.J.W.), Welch Foundation (F-2133-
778 20230405) (E.S.C.), and F.M. Jones and H.L. Bruce Graduate Fellowship (Z.W.).

779 **Data availability**

780 All relevant data can be found either within the article or in its supplementary information
781 section. Raw data is available upon request.

782 **Competing interests**

783 The authors declare no competing or financial interests.

784

785

786 **References**

787 1. Andrews-Zwilling, Y., Bien-Ly, N., Xu, Q., Li, G., Bernardo, A., Yoon, S. Y., Zwilling, D., Yan,
788 T. X., Chen, L., and Huang, Y. (2010). Apolipoprotein E4 causes age- and Tau-dependent
789 impairment of GABAergic interneurons, leading to learning and memory deficits in mice. *The*
790 *Journal of neuroscience : the official journal of the Society for Neuroscience*, *30*(41), 13707–
791 13717. https://doi.org/10.1523/JNEUROSCI.4040-10.2010
792 2. Aquino Nunez, W., Combs, B., Gamblin, T. C., and Ackley, B. D. (2022). Age-dependent
793 accumulation of tau aggregation in *Caenorhabditis elegans*. *Frontiers in aging*, *3*, 928574.
794 https://doi.org/10.3389/fragi.2022.928574
795 3. Arnold, M. L., Cooper, J., Grant, B. D., & Driscoll, M. (2020). Quantitative Approaches for
796 Scoring in vivo Neuronal Aggregate and Organelle Extrusion in Large Exopher Vesicles in
797 C. elegans. *Journal of visualized experiments : JoVE*, (163), 10.3791/61368.
798 https://doi.org/10.3791/61368
799 4. Asakura, T., Ogura, K., and Goshima, Y. (2007). UNC-6 expression by the vulval precursor
800 cells of Caenorhabditis elegans is required for the complex axon guidance of the HSN
801 neurons. *Developmental biology*, *304*(2), 800–810.
802 https://doi.org/10.1016/j.ydbio.2007.01.028
803 5. Avery, L., and Shtonda, B. B. (2003). Food transport in the C. elegans pharynx. *The Journal*
804 *of experimental biology*, *206*(Pt 14), 2441–2457. https://doi.org/10.1242/jeb.00433
805 6. Avery, L., and You, Y. J. (2012). C. elegans feeding. *WormBook : the online review of C.*
806 *elegans biology*, 1–23. https://doi.org/10.1895/wormbook.1.150.1
807 7. Baskoylu, S. N., Yersak, J., O'Hern, P., Grosser, S., Simon, J., Kim, S., Schuch, K.,
808 Dimitriadi, M., Yanagi, K. S., Lins, J., and Hart, A. C. (2018). Single copy/knock-in models of
809 ALS SOD1 in C. elegans suggest loss and gain of function have different contributions to
810 cholinergic and glutamatergic neurodegeneration. *PLoS genetics*, *14*(10), e1007682.
811 https://doi.org/10.1371/journal.pgen.1007682
812 8. Benbow, S. J., Strovas, T. J., Darvas, M., Saxton, A., and Kraemer, B. C. (2020). Synergistic
813 toxicity between tau and amyloid drives neuronal dysfunction and neurodegeneration in
814 transgenic C. elegans. *Human molecular genetics*, *29*(3), 495–505.
815 https://doi.org/10.1093/hmg/ddz319
816 9. Benzing, W. C., and Mufson, E. J. (1995). Apolipoprotein E immunoreactivity within
817 neurofibrillary tangles: relationship to Tau and PHF in Alzheimer's disease. *Experimental*
818 *neurology*, *132*(2), 162–171. https://doi.org/10.1016/0014-4886(95)90021-7
819 10. Bookheimer, S. Y., Strojwas, M. H., Cohen, M. S., Saunders, A. M., Pericak-Vance, M. A.,
820 Mazziotta, J. C., and Small, G. W. (2000). Patterns of brain activation in people at risk for
821 Alzheimer's disease. *The New England journal of medicine*, *343*(7), 450–456.
822 https://doi.org/10.1056/NEJM200008173430701

823 11. Braak, H., and Braak, E. (1991). Neuropathological stageing of Alzheimer-related changes.
824 *Acta neuropathologica*, *82*(4), 239–259. https://doi.org/10.1007/BF00308809
825 12. Braak, H., & Del Tredici, K. (2011). Alzheimer's pathogenesis: is there neuron-to-neuron
826 propagation?. *Acta neuropathologica*, *121*(5), 589–595. https://doi.org/10.1007/s00401-011-
827 0825-z
828 13. Brenner S. (1974). The genetics of Caenorhabditis elegans. *Genetics*, *77*(1), 71–94.
829 https://doi.org/10.1093/genetics/77.1.71
830 14. Brecht, W. J., Harris, F. M., Chang, S., Tesseur, I., Yu, G. Q., Xu, Q., Dee Fish, J., Wyss-
831 Coray, T., Buttini, M., Mucke, L., Mahley, R. W., and Huang, Y. (2004). Neuron-specific
832 apolipoprotein e4 proteolysis is associated with increased tau phosphorylation in brains of
833 transgenic mice. *The Journal of neuroscience : the official journal of the Society for*
834 *Neuroscience*, *24*(10), 2527–2534. https://doi.org/10.1523/JNEUROSCI.4315-03.2004
835 15. Butner, K. A., and Kirschner, M. W. (1991). Tau protein binds to microtubules through a
836 flexible array of distributed weak sites. *The Journal of cell biology*, *115*(3), 717–730.
837 https://doi.org/10.1083/jcb.115.3.717
838 16. Chalfie, M., and Sulston, J. (1981). Developmental genetics of the mechanosensory
839 neurons of Caenorhabditis elegans. *Developmental biology*, *82*(2), 358–370.
840 https://doi.org/10.1016/0012-1606(81)90459-0
841 17. Chalfie, M., and Thomson, J. N. (1979). Organization of neuronal microtubules in the
842 nematode Caenorhabditis elegans. *The Journal of cell biology*, *82*(1), 278–289.
843 https://doi.org/10.1083/jcb.82.1.278
844 18. Chalfie, M., and Thomson, J. N. (1982). Structural and functional diversity in the neuronal
845 microtubules of Caenorhabditis elegans. *The Journal of cell biology*, *93*(1), 15–23.
846 https://doi.org/10.1083/jcb.93.1.15
847 19. Chalfie, M., Sulston, J. E., White, J. G., Southgate, E., Thomson, J. N., and Brenner, S.
848 (1985). The neural circuit for touch sensitivity in Caenorhabditis elegans. *The Journal of*
849 *neuroscience : the official journal of the Society for Neuroscience*, *5*(4), 956–964.
850 https://doi.org/10.1523/JNEUROSCI.05-04-00956.1985
851 20. Chang, A. J., Chronis, N., Karow, D. S., Marletta, M. A., and Bargmann, C. I. (2006). A
852 distributed chemosensory circuit for oxygen preference in C. elegans. *PLoS biology*, *4*(9),
853 e274. https://doi.org/10.1371/journal.pbio.0040274
854 21. Clavaguera, F., Bolmont, T., Crowther, R. A., Abramowski, D., Frank, S., Probst, A., Fraser,
855 G., Stalder, A. K., Beibel, M., Staufenbiel, M., Jucker, M., Goedert, M., and Tolnay, M.
856 (2009). Transmission and spreading of tauopathy in transgenic mouse brain. *Nature cell*
857 *biology*, *11*(7), 909–913. https://doi.org/10.1038/ncb1901

858 22. Coakley, S., Ritchie, F. K., Galbraith, K. M., and Hilliard, M. A. (2020). Epidermal control of
859 axonal attachment via β-spectrin and the GTPase-activating protein TBC-10 prevents
860 axonal degeneration. *Nature communications*, *11*(1), 133. https://doi.org/10.1038/s41467-
861 019-13795-x
862 23. Cornblath, E. J., Li, H. L., Changolkar, L., Zhang, B., Brown, H. J., Gathagan, R. J., Olufemi,
863 M. F., Trojanowski, J. Q., Bassett, D. S., Lee, V. M. Y., and Henderson, M. X. (2021).
864 Computational modeling of tau pathology spread reveals patterns of regional vulnerability
865 and the impact of a genetic risk factor. *Science advances*, *7*(24), eabg6677.
866 https://doi.org/10.1126/sciadv.abg6677
867 24. Crespo-Biel, N., Theunis, C., Borghgraef, P., Lechat, B., Devijver, H., Maurin, H., and Van
868 Leuven, F. (2014). Phosphorylation of protein Tau by GSK3β prolongs survival of bigenic
869 Tau.P301L×GSK3β mice by delaying brainstem tauopathy. *Neurobiology of disease*, *67*,
870 119–132. https://doi.org/10.1016/j.nbd.2014.03.016
871 25. Daigle, I., and Li, C. (1993). apl-1, a Caenorhabditis elegans gene encoding a protein
872 related to the human beta-amyloid protein precursor. *Proceedings of the National Academy*
873 *of Sciences of the United States of America*, *90*(24), 12045–12049.
874 https://doi.org/10.1073/pnas.90.24.12045
875 26. Davis, A. A., Inman, C. E., Wargel, Z. M., Dube, U., Freeberg, B. M., Galluppi, A., Haines, J.
876 N., Dhavale, D. D., Miller, R., Choudhury, F. A., Sullivan, P. M., Cruchaga, C., Perlmutter, J.
877 S., Ulrich, J. D., Benitez, B. A., Kotzbauer, P. T., and Holtzman, D. M. (2020). *APOE*
878 genotype regulates pathology and disease progression in synucleinopathy. *Science*
879 *translational medicine*, *12*(529), eaay3069. https://doi.org/10.1126/scitranslmed.aay3069
880 27. de Calignon, A., Polydoro, M., Suárez-Calvet, M., William, C., Adamowicz, D. H., Kopeikina,
881 K. J., Pitstick, R., Sahara, N., Ashe, K. H., Carlson, G. A., Spires-Jones, T. L., and Hyman,
882 B. T. (2012). Propagation of tau pathology in a model of early Alzheimer's disease. *Neuron*,
883 *73*(4), 685–697. https://doi.org/10.1016/j.neuron.2011.11.033
884 28. DeVos, S. L., Miller, R. L., Schoch, K. M., Holmes, B. B., Kebodeaux, C. S., Wegener, A. J.,
885 Chen, G., Shen, T., Tran, H., Nichols, B., Zanardi, T. A., Kordasiewicz, H. B., Swayze, E. E.,
886 Bennett, C. F., Diamond, M. I., and Miller, T. M. (2017). Tau reduction prevents neuronal
887 loss and reverses pathological tau deposition and seeding in mice with tauopathy. *Science*
888 *translational medicine*, *9*(374), eaag0481. https://doi.org/10.1126/scitranslmed.aag0481
889 29. Eichel, K., Uenaka, T., Belapurkar, V., Lu, R., Cheng, S., Pak, J. S., Taylor, C. A., Südhof, T.
890 C., Malenka, R., Wernig, M., Özkan, E., Perrais, D., and Shen, K. (2022). Endocytosis in the
891 axon initial segment maintains neuronal polarity. *Nature*, *609*(7925), 128–135.
892 https://doi.org/10.1038/s41586-022-05074-5

30. Esposito, G., Di Schiavi, E., Bergamasco, C., and Bazzicalupo, P. (2007). Efficient and cell specific knock-down of gene function in targeted C. elegans neurons. *Gene*, *395*(1-2), 170–176. https://doi.org/10.1016/j.gene.2007.03.002
31. Faber, P. W., Alter, J. R., MacDonald, M. E., and Hart, A. C. (1999). Polyglutamine-mediated dysfunction and apoptotic death of a Caenorhabditis elegans sensory neuron. *Proceedings of the National Academy of Sciences of the United States of America*, *96*(1), 179–184. https://doi.org/10.1073/pnas.96.1.179
32. Fatouros, C., Pir, G. J., Biernat, J., Koushika, S. P., Mandelkow, E., Mandelkow, E. M., Schmidt, E., and Baumeister, R. (2012). Inhibition of tau aggregation in a novel Caenorhabditis elegans model of tauopathy mitigates proteotoxicity. *Human molecular genetics*, *21*(16), 3587–3603. https://doi.org/10.1093/hmg/dds190
33. Fiford, C. M., Ridgway, G. R., Cash, D. M., Modat, M., Nicholas, J., Manning, E. N., Malone, I. B., Biessels, G. J., Ourselin, S., Carmichael, O. T., Cardoso, M. J., Barnes, J., and Alzheimer's Disease Neuroimaging Initiative (2018). Patterns of progressive atrophy vary with age in Alzheimer's disease patients. *Neurobiology of aging*, *63*, 22–32. https://doi.org/10.1016/j.neurobiolaging.2017.11.002
34. Flavell, S. W., Raizen, D. M., and You, Y. J. (2020). Behavioral States. *Genetics*, *216*(2), 315–332. https://doi.org/10.1534/genetics.120.303539
35. Fortea, J., Pegueroles, J., Alcolea, D., Belbin, O., Dols-Icardo, O., Vaqué-Alcázar, L., Videla, L., Gispert, J. D., Suárez-Calvet, M., Johnson, S. C., Sperling, R., Bejanin, A., Lleó, A., and Montal, V. (2024). APOE4 homozygozity represents a distinct genetic form of Alzheimer's disease. *Nature medicine*, *30*(5), 1284–1291. https://doi.org/10.1038/s41591-024-02931-w
36. Friedhoff, P., Schneider, A., Mandelkow, E. M., and Mandelkow, E. (1998). Rapid assembly of Alzheimer-like paired helical filaments from microtubule-associated protein tau monitored by fluorescence in solution. *Biochemistry*, *37*(28), 10223–10230. https://doi.org/10.1021/bi980537d
37. Friedhoff, P., von Bergen, M., Mandelkow, E. M., Davies, P., and Mandelkow, E. (1998). A nucleated assembly mechanism of Alzheimer paired helical filaments. *Proceedings of the National Academy of Sciences of the United States of America*, *95*(26), 15712–15717. https://doi.org/10.1073/pnas.95.26.15712
38. Frøkjaer-Jensen, C., Davis, M. W., Hopkins, C. E., Newman, B. J., Thummel, J. M., Olesen, S. P., Grunnet, M., and Jorgensen, E. M. (2008). Single-copy insertion of transgenes in Caenorhabditis elegans. *Nature genetics*, *40*(11), 1375–1383. https://doi.org/10.1038/ng.248
39. Frost, B., and Diamond, M. I. (2010). Prion-like mechanisms in neurodegenerative diseases. *Nature reviews. Neuroscience*, *11*(3), 155–159. https://doi.org/10.1038/nrn2786

929 40. Fu, H., Hussaini, S. A., Wegmann, S., Profaci, C., Daniels, J. D., Herman, M., Emrani, S.,
930 Figueroa, H. Y., Hyman, B. T., Davies, P., and Duff, K. E. (2016). 3D Visualization of the
931 Temporal and Spatial Spread of Tau Pathology Reveals Extensive Sites of Tau
932 Accumulation Associated with Neuronal Loss and Recognition Memory Deficit in Aged Tau
933 Transgenic Mice. *PloS one*, *11*(7), e0159463. https://doi.org/10.1371/journal.pone.0159463
934 41. Fujiwara M, Ishihara T, Katsura I. (1999). A novel WD40 protein, CHE-2, acts cell-
935 autonomously in the formation of *C. elegans* sensory cilia. *Development*. 126(21):4839-48.
936 https://doi: 10.1242/dev.126.21.4839.
937 42. Gao, S., Guan, S. A., Fouad, A. D., Meng, J., Kawano, T., Huang, Y. C., Li, Y., Alcaire, S.,
938 Hung, W., Lu, Y., Qi, Y. B., Jin, Y., Alkema, M., Fang-Yen, C., and Zhen, M. (2018).
939 Excitatory motor neurons are local oscillators for backward locomotion. *eLife*, *7*, e29915.
940 https://doi.org/10.7554/eLife.29915
941 43. Garriga, G., Desai, C., and Horvitz, H. R. (1993). Cell interactions control the direction of
942 outgrowth, branching and fasciculation of the HSN axons of Caenorhabditis elegans.
943 *Development (Cambridge, England)*, *117*(3), 1071–1087.
944 https://doi.org/10.1242/dev.117.3.1071
945 44. Ghoshal, N., García-Sierra, F., Wuu, J., Leurgans, S., Bennett, D. A., Berry, R. W., and
946 Binder, L. I. (2002). Tau conformational changes correspond to impairments of episodic
947 memory in mild cognitive impairment and Alzheimer's disease. *Experimental neurology*,
948 *177*(2), 475–493. https://doi.org/10.1006/exnr.2002.8014
949 45. Goedert, M., Baur, C. P., Ahringer, J., Jakes, R., Hasegawa, M., Spillantini, M. G., Smith, M.
950 J., and Hill, F. (1996). PTL-1, a microtubule-associated protein with tau-like repeats from the
951 nematode Caenorhabditis elegans. *Journal of cell science*, *109 (Pt 11)*, 2661–2672.
952 https://doi.org/10.1242/jcs.109.11.2661
953 46. Gordon, P., Hingula, L., Krasny, M. L., Swienckowski, J. L., Pokrywka, N. J., and Raley-
954 Susman, K. M. (2008). The invertebrate microtubule-associated protein PTL-1 functions in
955 mechanosensation and development in Caenorhabditis elegans. *Development genes and*
956 *evolution*, *218*(10), 541–551. https://doi.org/10.1007/s00427-008-0250-z
957 47. Grundke-Iqbal, I., Iqbal, K., Quinlan, M., Tung, Y. C., Zaidi, M. S., and Wisniewski, H. M.
958 (1986). Microtubule-associated protein tau. A component of Alzheimer paired helical
959 filaments. *The Journal of biological chemistry*, *261*(13), 6084–6089.
960 48. Harterink, M., Edwards, S. L., de Haan, B., Yau, K. W., van den Heuvel, S., Kapitein, L. C.,
961 Miller, K. G., and Hoogenraad, C. C. (2018). Local microtubule organization promotes cargo
962 transport in *C. elegans* dendrites. *Journal of cell science*, *131*(20), jcs223107.
963 https://doi.org/10.1242/jcs.223107

964 49. Hashi, Y., Kotani, S., and Adachi, T. (2016). A nematode microtubule-associated protein,
965 PTL-1, closely resembles its mammalian counterparts in overall molecular architecture.
966 *Bioscience, Biotechnology, and Biochemistry*, *80*(6), 1107–1113.
967 https://doi.org/10.1080/09168451.2016.1141038
968 50. Horvitz H. R. (2003). Worms, life, and death (Nobel lecture). *Chembiochem : a European*
969 *journal of chemical biology*, *4*(8), 697–711. https://doi.org/10.1002/cbic.200300614
970 51. Huang, Y., Liu, X. Q., Wyss-Coray, T., Brecht, W. J., Sanan, D. A., and Mahley, R. W.
971 (2001). Apolipoprotein E fragments present in Alzheimer's disease brains induce
972 neurofibrillary tangle-like intracellular inclusions in neurons. *Proceedings of the National*
973 *Academy of Sciences of the United States of America*, *98*(15), 8838–8843.
974 https://doi.org/10.1073/pnas.151254698
975 52. Iba, M., Guo, J. L., McBride, J. D., Zhang, B., Trojanowski, J. Q., and Lee, V. M. (2013).
976 Synthetic tau fibrils mediate transmission of neurofibrillary tangles in a transgenic mouse
977 model of Alzheimer's-like tauopathy. *The Journal of neuroscience : the official journal of the*
978 *Society for Neuroscience*, *33*(3), 1024–1037. https://doi.org/10.1523/JNEUROSCI.2642-
979 12.2013
980 53. Izquierdo, E. J., and Beer, R. D. (2018). From head to tail: a neuromechanical model of
981 forward locomotion in *Caenorhabditis elegans*. *Philosophical transactions of the Royal*
982 *Society of London. Series B, Biological sciences*, *373*(1758), 20170374.
983 https://doi.org/10.1098/rstb.2017.0374
984 54. Jeganathan, S., Hascher, A., Chinnathambi, S., Biernat, J., Mandelkow, E. M., and
985 Mandelkow, E. (2008). Proline-directed pseudo-phosphorylation at AT8 and PHF1 epitopes
986 induces a compaction of the paperclip folding of Tau and generates a pathological (MC-1)
987 conformation. *The Journal of biological chemistry*, *283*(46), 32066–32076.
988 https://doi.org/10.1074/jbc.M805300200
989 55. Jeganathan, S., von Bergen, M., Brutlach, H., Steinhoff, H. J., and Mandelkow, E. (2006).
990 Global hairpin folding of tau in solution. *Biochemistry*, *45*(7), 2283–2293.
991 https://doi.org/10.1021/bi0521543
992 56. Jiang, W. I., Cao, Y., Xue, Y., Ji, Y., Winer, B. Y., Chandra, R., Zhang, X. F., Zhang, M.,
993 Singhal, N. S., Pierce, J. T., Chen, S., and Ma, D. K. (2025). Suppressing APOE4-induced
994 neural pathologies by targeting the VHL-HIF axis. *Proceedings of the National Academy of*
995 *Sciences of the United States of America*, *122*(5), e2417515122.
996 https://doi.org/10.1073/pnas.2417515122
997 57. Kfoury, N., Holmes, B. B., Jiang, H., Holtzman, D. M., and Diamond, M. I. (2012). Trans-
998 cellular propagation of Tau aggregation by fibrillar species. *The Journal of biological*
999 *chemistry*, *287*(23), 19440–19451. https://doi.org/10.1074/jbc.M112.346072

1000 58. Köpke, E., Tung, Y. C., Shaikh, S., Alonso, A. C., Iqbal, K., and Grundke-Iqbal, I. (1993).
1001 Microtubule-associated protein tau. Abnormal phosphorylation of a non-paired helical
1002 filament pool in Alzheimer disease. *The Journal of biological chemistry*, *268*(32), 24374–
1003 24384.
1004 59. Koriath, C., Lashley, T., Taylor, W., Druyeh, R., Dimitriadis, A., Denning, N., Williams, J.,
1005 Warren, J. D., Fox, N. C., Schott, J. M., Rowe, J. B., Collinge, J., Rohrer, J. D., and Mead,
1006 S. (2019). ApoE4 lowers age at onset in patients with frontotemporal dementia and
1007 tauopathy independent of amyloid-β copathology. *Alzheimer's and dementia (Amsterdam,*
1008 *Netherlands)*, *11*, 277–280. https://doi.org/10.1016/j.dadm.2019.01.010
1009 60. Kosik, K. S., Orecchio, L. D., Binder, L., Trojanowski, J. Q., Lee, V. M., and Lee, G. (1988).
1010 Epitopes that span the tau molecule are shared with paired helical filaments. *Neuron*, *1*(9),
1011 817–825. https://doi.org/10.1016/0896-6273(88)90129-8
1012 61. Koutsodendris, N., Blumenfeld, J., Agrawal, A., Traglia, M., Grone, B., Zilberter, M., Yip, O.,
1013 Rao, A., Nelson, M. R., Hao, Y., Thomas, R., Yoon, S. Y., Arriola, P., and Huang, Y. (2023).
1014 Neuronal APOE4 removal protects against tau-mediated gliosis, neurodegeneration and
1015 myelin deficits. *Nature aging*, *3*(3), 275–296. https://doi.org/10.1038/s43587-023-00368-3
1016 62. Kowall, N. W., and Kosik, K. S. (1987). Axonal disruption and aberrant localization of tau
1017 protein characterize the neuropil pathology of Alzheimer's disease. *Annals of neurology*,
1018 *22*(5), 639–643. https://doi.org/10.1002/ana.410220514
1019 63. Kraemer, B. C., Zhang, B., Leverenz, J. B., Thomas, J. H., Trojanowski, J. Q., and
1020 Schellenberg, G. D. (2003). Neurodegeneration and defective neurotransmission in a
1021 Caenorhabditis elegans model of tauopathy. *Proceedings of the National Academy of*
1022 *Sciences of the United States of America*, *100*(17), 9980–9985.
1023 https://doi.org/10.1073/pnas.1533448100
1024 64. Krieg, M., Stühmer, J., Cueva, J. G., Fetter, R., Spilker, K., Cremers, D., Shen, K., Dunn, A.
1025 R., and Goodman, M. B. (2017). Genetic defects in β-spectrin and tau sensitize *C. elegans*
1026 axons to movement-induced damage via torque-tension coupling. *eLife*, *6*, e20172.
1027 https://doi.org/10.7554/eLife.20172
1028 65. Larsen, F. K., Baksh, R. A., McGlinchey, E., Langballe, E. M., Benejam, B., Beresford-
1029 Webb, J., McCarron, M., Coppus, A., Falquero, S., Fortea, J., Levin, J., Loosli, S. V., Mark,
1030 R., Rebillat, A. S., Zaman, S., and Strydom, A. (2024). Age of Alzheimer's disease diagnosis
1031 in people with Down syndrome and associated factors: Results from the Horizon 21
1032 European Down syndrome consortium. *Alzheimer's and dementia : the journal of the*
1033 *Alzheimer's Association*, *20*(5), 3270–3280. https://doi.org/10.1002/alz.13779
1034 66. Lee, S., Viqar, F., Zimmerman, M. E., Narkhede, A., Tosto, G., Benzinger, T. L., Marcus, D.
1035 S., Fagan, A. M., Goate, A., Fox, N. C., Cairns, N. J., Holtzman, D. M., Buckles, V., Ghetti,

1036 B., McDade, E., Martins, R. N., Saykin, A. J., Masters, C. L., Ringman, J. M., Ryan, N. S., …
1037 Dominantly Inherited Alzheimer Network (2016). White matter hyperintensities are a core
1038 feature of Alzheimer's disease: Evidence from the dominantly inherited Alzheimer network.
1039 *Annals of neurology*, *79*(6), 929–939. https://doi.org/10.1002/ana.24647
1040 67. Lee, V. M., and Trojanowski, J. Q. (1992). The disordered neuronal cytoskeleton in
1041 Alzheimer's disease. *Current opinion in neurobiology*, *2*(5), 653–656.
1042 https://doi.org/10.1016/0959-4388(92)90034-i
1043 68. Leroy, K., Yilmaz, Z., and Brion, J. P. (2007). Increased level of active GSK-3beta in
1044 Alzheimer's disease and accumulation in argyrophilic grains and in neurones at different
1045 stages of neurofibrillary degeneration. *Neuropathology and applied neurobiology*, *33*(1), 43–
1046 55. https://doi.org/10.1111/j.1365-2990.2006.00795.x
1047 69. Li, W., Kang, L., Piggott, B. J., Feng, Z., and Xu, X. Z. (2011). The neural circuits and
1048 sensory channels mediating harsh touch sensation in Caenorhabditis elegans. *Nature*
1049 *communications*, *2*, 315. https://doi.org/10.1038/ncomms1308
1050 70. Lima-Silva, T. B., Bahia, V. S., Carvalho, V. A., Guimarães, H. C., Caramelli, P., Balthazar,
1051 M., Damasceno, B., Bottino, C. M. C., Brucki, S. M. D., Nitrini, R., and Yassuda, M. S.
1052 (2013). Functional profile of patients with behavioral variant frontotemporal dementia
1053 (bvFTD) compared to patients with Alzheimer's disease and normal controls. *Dementia and*
1054 *neuropsychologia*, *7*(1), 96–103. https://doi.org/10.1590/S1980-57642013DN70100015
1055 71. Lin, L. C., Nana, A. L., Hepker, M., Hwang, J. L., Gaus, S. E., Spina, S., Cosme, C. G., Gan,
1056 L., Grinberg, L. T., Geschwind, D. H., Coppola, G., Rosen, H. J., Miller, B. L., and Seeley,
1057 W. W. (2019). Preferential tau aggregation in von Economo neurons and fork cells in
1058 frontotemporal lobar degeneration with specific MAPT variants. *Acta neuropathologica*
1059 *communications*, *7*(1), 159. https://doi.org/10.1186/s40478-019-0809-0
1060 72. Liu, L., Drouet, V., Wu, J. W., Witter, M. P., Small, S. A., Clelland, C., and Duff, K. (2012).
1061 Trans-synaptic spread of tau pathology in vivo. *PloS one*, *7*(2), e31302.
1062 https://doi.org/10.1371/journal.pone.0031302
1063 73. McCulloch, K. A., Qi, Y. B., Takayanagi-Kiya, S., Jin, Y., and Cherra, S. J., 3rd (2017). Novel
1064 Mutations in Synaptic Transmission Genes Suppress Neuronal Hyperexcitation in
1065 *Caenorhabditis elegans*. *G3 (Bethesda, Md.)*, *7*(7), 2055–2063.
1066 https://doi.org/10.1534/g3.117.042598
1067 74. McDermott, J. B., Aamodt, S., and Aamodt, E. (1996). ptl-1, a Caenorhabditis elegans gene
1068 whose products are homologous to the tau microtubule-associated proteins. *Biochemistry*,
1069 *35*(29), 9415–9423. https://doi.org/10.1021/bi952646n
1070 75. Meijering, E., Jacob, M., Sarria, J. C., Steiner, P., Hirling, H., and Unser, M. (2004). Design
1071 and validation of a tool for neurite tracing and analysis in fluorescence microscopy images.

1072 *Cytometry. Part A : the journal of the International Society for Analytical Cytology*, *58*(2),
1073 167–176. https://doi.org/10.1002/cyto.a.20022
1074 76. Meisl, G., Hidari, E., Allinson, K., Rittman, T., DeVos, S. L., Sanchez, J. S., Xu, C. K., Duff,
1075 K. E., Johnson, K. A., Rowe, J. B., Hyman, B. T., Knowles, T. P. J., and Klenerman, D.
1076 (2021). In vivo rate-determining steps of tau seed accumulation in Alzheimer's disease.
1077 *Science advances*, *7*(44), eabh1448. https://doi.org/10.1126/sciadv.abh1448
1078 77. Miller, K. G., Alfonso, A., Nguyen, M., Crowell, J. A., Johnson, C. D., and Rand, J. B. (1996).
1079 A genetic selection for Caenorhabditis elegans synaptic transmission mutants. *Proceedings*
1080 *of the National Academy of Sciences of the United States of America*, *93*(22), 12593–12598.
1081 https://doi.org/10.1073/pnas.93.22.12593
1082 78. Mitchell, D. H., Stiles, J. W., Santelli, J., and Sanadi, D. R. (1979). Synchronous growth and
1083 aging of Caenorhabditis elegans in the presence of fluorodeoxyuridine. *Journal of*
1084 *gerontology*, *34*(1), 28–36. https://doi.org/10.1093/geronj/34.1.28
1085 79. Mizumoto, K., and Shen, K. (2013). Interaxonal interaction defines tiled presynaptic
1086 innervation in C. elegans. *Neuron*, *77*(4), 655–666.
1087 https://doi.org/10.1016/j.neuron.2012.12.031
1088 80. Mocanu, M. M., Nissen, A., Eckermann, K., Khlistunova, I., Biernat, J., Drexler, D., Petrova,
1089 O., Schönig, K., Bujard, H., Mandelkow, E., Zhou, L., Rune, G., and Mandelkow, E. M.
1090 (2008). The potential for beta-structure in the repeat domain of tau protein determines
1091 aggregation, synaptic decay, neuronal loss, and coassembly with endogenous Tau in
1092 inducible mouse models of tauopathy. *The Journal of neuroscience : the official journal of*
1093 *the Society for Neuroscience*, *28*(3), 737–748. https://doi.org/10.1523/JNEUROSCI.2824-
1094 07.2008
1095 81. Natale, C., Barzago, M. M., and Diomede, L. (2020). *Caenorhabditis elegans* Models to
1096 Investigate the Mechanisms Underlying Tau Toxicity in Tauopathies. *Brain sciences*, *10*(11),
1097 838. https://doi.org/10.3390/brainsci10110838
1098 82. Nikoletopoulou, V., and Tavernarakis, N. (2014). Necrotic cell death in Caenorhabditis
1099 elegans. *Methods in enzymology*, *545*, 127–155. https://doi.org/10.1016/B978-0-12-801430-
1100 1.00006-8
1101 83. Nordquist, S. K., Smith, S. R., and Pierce, J. T. (2018). Systematic Functional
1102 Characterization of Human 21st Chromosome Orthologs in *Caenorhabditis elegans*. *G3*
1103 *(Bethesda, Md.)*, *8*(3), 967–979. https://doi.org/10.1534/g3.118.200019
1104 84. Nuriel, T., Angulo, S. L., Khan, U., Ashok, A., Chen, Q., Figueroa, H. Y., Emrani, S., Liu, L.,
1105 Herman, M., Barrett, G., Savage, V., Buitrago, L., Cepeda-Prado, E., Fung, C., Goldberg, E.,
1106 Gross, S. S., Hussaini, S. A., Moreno, H., Small, S. A., and Duff, K. E. (2017). Neuronal

1107 hyperactivity due to loss of inhibitory tone in APOE4 mice lacking Alzheimer's disease-like
1108 pathology. *Nature communications*, *8*(1), 1464. https://doi.org/10.1038/s41467-017-01444-0
1109 85. Oakley, S. S., Maina, M. B., Marshall, K. E., Al-Hilaly, Y. K., Harrington, C. R., Wischik, C.
1110 M., and Serpell, L. C. (2020). Tau Filament Self-Assembly and Structure: Tau as a
1111 Therapeutic Target. *Frontiers in neurology*, *11*, 590754.
1112 https://doi.org/10.3389/fneur.2020.590754
1113 86. O'Hagan, R., Chalfie, M., and Goodman, M. B. (2005). The MEC-4 DEG/ENaC channel of
1114 Caenorhabditis elegans touch receptor neurons transduces mechanical signals. *Nature*
1115 *neuroscience*, *8*(1), 43–50. https://doi.org/10.1038/nn1362
1116 87. Pan CL, Peng CY, Chen CH, McIntire S. Genetic analysis of age-dependent defects of the
1117 Caenorhabditis elegans touch receptor neurons. Proc Natl Acad Sci U S A. 2011 May
1118 31;108(22):9274-9. doi: 10.1073/pnas.1011711108. Epub 2011 May 12. PMID: 21571636;
1119 PMCID: PMC3107274.
1120 88. Rietdijk, C. D., Perez-Pardo, P., Garssen, J., van Wezel, R. J., and Kraneveld, A. D. (2017).
1121 Exploring Braak's Hypothesis of Parkinson's Disease. *Frontiers in neurology*, *8*, 37.
1122 https://doi.org/10.3389/fneur.2017.00037
1123 89. Roberson, E. D., Scearce-Levie, K., Palop, J. J., Yan, F., Cheng, I. H., Wu, T., Gerstein, H.,
1124 Yu, G. Q., and Mucke, L. (2007). Reducing endogenous tau ameliorates amyloid beta-
1125 induced deficits in an Alzheimer's disease mouse model. *Science (New York, N.Y.)*,
1126 *316*(5825), 750–754. https://doi.org/10.1126/science.1141736
1127 90. Robinson, J. L., Lee, E. B., Xie, S. X., Rennert, L., Suh, E., Bredenberg, C., Caswell, C.,
1128 Van Deerlin, V. M., Yan, N., Yousef, A., Hurtig, H. I., Siderowf, A., Grossman, M., McMillan,
1129 C. T., Miller, B., Duda, J. E., Irwin, D. J., Wolk, D., Elman, L., McCluskey, L., … Trojanowski,
1130 J. Q. (2018). Neurodegenerative disease concomitant proteinopathies are prevalent, age-
1131 related and APOE4-associated. *Brain : a journal of neurology*, *141*(7), 2181–2193.
1132 https://doi.org/10.1093/brain/awy146
1133 91. Rohn, T. T., Catlin, L. W., Coonse, K. G., and Habig, J. W. (2012). Identification of an
1134 amino-terminal fragment of apolipoprotein E4 that localizes to neurofibrillary tangles of the
1135 Alzheimer's disease brain. *Brain research*, *1475*, 106–115.
1136 https://doi.org/10.1016/j.brainres.2012.08.003
1137 92. Rondina, J. M., Ferreira, L. K., de Souza Duran, F. L., Kubo, R., Ono, C. R., Leite, C. C.,
1138 Smid, J., Nitrini, R., Buchpiguel, C. A., and Busatto, G. F. (2017). Selecting the most
1139 relevant brain regions to discriminate Alzheimer's disease patients from healthy controls
1140 using multiple kernel learning: A comparison across functional and structural imaging
1141 modalities and atlases. *NeuroImage. Clinical*, *17*, 628–641.
1142 https://doi.org/10.1016/j.nicl.2017.10.026

1143 93. Rosen, H. J., Allison, S. C., Schauer, G. F., Gorno-Tempini, M. L., Weiner, M. W., and Miller,
1144 B. L. (2005). Neuroanatomical correlates of behavioural disorders in dementia. *Brain : a*
1145 *journal of neurology*, *128*(Pt 11), 2612–2625. https://doi.org/10.1093/brain/awh628
1146 94. Roux, A. E., Yuan, H., Podshivalova, K., Hendrickson, D., Kerr, R., Kenyon, C., and Kelley,
1147 D. (2023). Individual cell types in C. elegans age differently and activate distinct cell-
1148 protective responses. *Cell reports*, *42*(8), 112902.
1149 https://doi.org/10.1016/j.celrep.2023.112902
1150 95. Ryan, N. S., and Rossor, M. N. (2010). Correlating familial Alzheimer's disease gene
1151 mutations with clinical phenotype. *Biomarkers in medicine*, *4*(1), 99–112.
1152 https://doi.org/10.2217/bmm.09.92
1153 96. Sae-Lee, W., Scott, L. L., Brose, L., Encarnacion, A. J., Shi, T., Kore, P., Oyibo, L. O., Ye,
1154 C., Rozmiarek, S. K., and Pierce, J. T. (2020). *APP*-Induced Patterned Neurodegeneration
1155 Is Exacerbated by *APOE4* in *Caenorhabditis elegans*. *G3 (Bethesda, Md.)*, *10*(8), 2851–
1156 2861. https://doi.org/10.1534/g3.120.401486
1157 97. Sanfeliu-Cerdán, N., Català-Castro, F., Mateos, B., Garcia-Cabau, C., Ribera, M., Ruider, I.,
1158 Porta-de-la-Riva, M., Canals-Calderón, A., Wieser, S., Salvatella, X., and Krieg, M. (2023).
1159 A MEC-2/stomatin condensate liquid-to-solid phase transition controls neuronal
1160 mechanotransduction during touch sensing. *Nature cell biology*, *25*(11), 1590–1599.
1161 https://doi.org/10.1038/s41556-023-01247-0
1162 98. Santarella, R. A., Skiniotis, G., Goldie, K. N., Tittmann, P., Gross, H., Mandelkow, E. M.,
1163 Mandelkow, E., and Hoenger, A. (2004). Surface-decoration of microtubules by human tau.
1164 *Journal of molecular biology*, *339*(3), 539–553. https://doi.org/10.1016/j.jmb.2004.04.008
1165 99. Scahill, R. I., Schott, J. M., Stevens, J. M., Rossor, M. N., and Fox, N. C. (2002). Mapping
1166 the evolution of regional atrophy in Alzheimer's disease: unbiased analysis of fluid-
1167 registered serial MRI. *Proceedings of the National Academy of Sciences of the United*
1168 *States of America*, *99*(7), 4703–4707. https://doi.org/10.1073/pnas.052587399
1169 100. Schafer W. R. (2005). Egg-laying. *WormBook : the online review of C. elegans biology*,
1170 1–7. https://doi.org/10.1895/wormbook.1.38.1
1171 101. Scharf, A., Pohl, F., Egan, B. M., Kocsisova, Z., and Kornfeld, K. (2021). Reproductive
1172 Aging in *Caenorhabditis elegans*: From Molecules to Ecology. *Frontiers in cell and*
1173 *developmental biology*, *9*, 718522. https://doi.org/10.3389/fcell.2021.718522
1174 102. Schneider, C. A., Rasband, W. S., and Eliceiri, K. W. (2012). NIH Image to ImageJ: 25
1175 years of image analysis. *Nature Methods*, *9*(7), 671–675. doi:10.1038/nmeth.2089
1176 103. Seo, D. O., O'Donnell, D., Jain, N., Ulrich, J. D., Herz, J., Li, Y., Lemieux, M., Cheng, J.,
1177 Hu, H., Serrano, J. R., Bao, X., Franke, E., Karlsson, M., Meier, M., Deng, S., Desai, C.,
1178 Dodiya, H., Lelwala-Guruge, J., Handley, S. A., Kipnis, J., … Holtzman, D. M. (2023). ApoE

1179 isoform- and microbiota-dependent progression of neurodegeneration in a mouse model of
1180 tauopathy. *Science (New York, N.Y.)*, *379*(6628), eadd1236.
1181 https://doi.org/10.1126/science.add1236
1182 104. Serrano-Pozo, A., Das, S., and Hyman, B. T. (2021). APOE and Alzheimer's disease:
1183 advances in genetics, pathophysiology, and therapeutic approaches. *The Lancet.*
1184 *Neurology*, *20*(1), 68–80. https://doi.org/10.1016/S1474-4422(20)30412-9
1185 105. Shi, Y., Yamada, K., Liddelow, S. A., Smith, S. T., Zhao, L., Luo, W., Tsai, R. M., Spina,
1186 S., Grinberg, L. T., Rojas, J. C., Gallardo, G., Wang, K., Roh, J., Robinson, G., Finn, M. B.,
1187 Jiang, H., Sullivan, P. M., Baufeld, C., Wood, M. W., Sutphen, C., … Holtzman, D. M.
1188 (2017). ApoE4 markedly exacerbates tau-mediated neurodegeneration in a mouse model of
1189 tauopathy. *Nature*, *549*(7673), 523–527. https://doi.org/10.1038/nature24016
1190 106. Spittaels, K., Van den Haute, C., Van Dorpe, J., Bruynseels, K., Vandezande, K.,
1191 Laenen, I., Geerts, H., Mercken, M., Sciot, R., Van Lommel, A., Loos, R., and Van Leuven,
1192 F. (1999). Prominent axonopathy in the brain and spinal cord of transgenic mice
1193 overexpressing four-repeat human tau protein. *The American journal of pathology*, *155*(6),
1194 2153–2165. https://doi.org/10.1016/S0002-9440(10)65533-2
1195 107. Steciuk, M., Cheong, M., Waite, C., You, Y. J., and Avery, L. (2014). Regulation of
1196 synaptic transmission at the Caenorhabditis elegans M4 neuromuscular junction by an
1197 antagonistic relationship between two calcium channels. *G3 (Bethesda, Md.)*, *4*(12), 2535–
1198 2543. https://doi.org/10.1534/g3.114.014308
1199 108. Strang, K. H., Golde, T. E., and Giasson, B. I. (2019). MAPT mutations, tauopathy, and
1200 mechanisms of neurodegeneration. *Laboratory investigation; a journal of technical methods*
1201 *and pathology*, *99*(7), 912–928. https://doi.org/10.1038/s41374-019-0197-x
1202 109. Sündermann, F., Fernandez, M. P., and Morgan, R. O. (2016). An evolutionary roadmap
1203 to the microtubule-associated protein MAP Tau. *BMC genomics*, *17*, 264.
1204 https://doi.org/10.1186/s12864-016-2590-9
1205 110. Taylor, S. R., Santpere, G., Weinreb, A., Barrett, A., Reilly, M. B., Xu, C., Varol, E.,
1206 Oikonomou, P., Glenwinkel, L., McWhirter, R., Poff, A., Basavaraju, M., Rafi, I., Yemini, E.,
1207 Cook, S. J., Abrams, A., Vidal, B., Cros, C., Tavazoie, S., Sestan, N., … Miller, D. M., 3rd
1208 (2021). Molecular topography of an entire nervous system. *Cell*, *184*(16), 4329–4347.e23.
1209 https://doi.org/10.1016/j.cell.2021.06.023
1210 111. Therriault, J., Benedet, A. L., Pascoal, T. A., Mathotaarachchi, S., Chamoun, M., Savard,
1211 M., Thomas, E., Kang, M. S., Lussier, F., Tissot, C., Parsons, M., Qureshi, M. N. I., Vitali, P.,
1212 Massarweh, G., Soucy, J. P., Rej, S., Saha-Chaudhuri, P., Gauthier, S., and Rosa-Neto, P.
1213 (2020). Association of Apolipoprotein E ε4 With Medial Temporal Tau Independent of
1214 Amyloid-β. *JAMA neurology*, *77*(4), 470–479. https://doi.org/10.1001/jamaneurol.2019.4421

1215 112. Topalidou, I., Chen, P. A., Cooper, K., Watanabe, S., Jorgensen, E. M., and Ailion, M.
1216 (2017). The NCA-1 and NCA-2 Ion Channels Function Downstream of G_q and Rho To
1217 Regulate Locomotion in *Caenorhabditis elegans*. *Genetics*, *206*(1), 265–282.
1218 https://doi.org/10.1534/genetics.116.198820
1219 113. Trent, C., Tsung, N., and Horvitz, H. R. (1983). Egg-laying defective mutants of the
1220 nematode Caenorhabditis elegans. *Genetics*, *104*(4), 619–647.
1221 https://doi.org/10.1093/genetics/104.4.619
1222 114. Trent, C., Tsung, N., and Horvitz, H. R. (1983). Egg-laying defective mutants of the
1223 nematode Caenorhabditis elegans. *Genetics*, *104*(4), 619–647.
1224 https://doi.org/10.1093/genetics/104.4.619
1225 115. Treusch, S., Hamamichi, S., Goodman, J. L., Matlack, K. E., Chung, C. Y., Baru, V.,
1226 Shulman, J. M., Parrado, A., Bevis, B. J., Valastyan, J. S., Han, H., Lindhagen-Persson, M.,
1227 Reiman, E. M., Evans, D. A., Bennett, D. A., Olofsson, A., DeJager, P. L., Tanzi, R. E.,
1228 Caldwell, K. A., Caldwell, G. A., … Lindquist, S. (2011). Functional links between Aβ toxicity,
1229 endocytic trafficking, and Alzheimer's disease risk factors in yeast. *Science (New York,*
1230 *N.Y.)*, *334*(6060), 1241–1245. https://doi.org/10.1126/science.1213210
1231 116. Trojanowski, J. Q., Schmidt, M. L., Shin, R. W., Bramblett, G. T., Rao, D., and Lee, V. M.
1232 (1993). Altered tau and neurofilament proteins in neuro-degenerative diseases: diagnostic
1233 implications for Alzheimer's disease and Lewy body dementias. *Brain pathology (Zurich,*
1234 *Switzerland)*, *3*(1), 45–54. https://doi.org/10.1111/j.1750-3639.1993.tb00725.x
1235 117. Tsutsui, K., Kim, H. S., Yoshikata, C., Kimura, K., Kubota, Y., Shibata, Y., Tian, C., Liu,
1236 J., and Nishiwaki, K. (2021). Repulsive guidance molecule acts in axon branching in
1237 Caenorhabditis elegans. *Scientific reports*, *11*(1), 22370. https://doi.org/10.1038/s41598-
1238 021-01853-8
1239 118. Tuovinen, T., Kananen, J., Rajna, Z., Lieslehto, J., Korhonen, V., Rytty, R., Mattila, H.,
1240 Huotari, N., Raitamaa, L., Helakari, H., Elseoud, A. A., Krüger, J., LeVan, P., Tervonen, O.,
1241 Hennig, J., Remes, A. M., Nedergaard, M., and Kiviniemi, V. (2020). The variability of
1242 functional MRI brain signal increases in Alzheimer's disease at cardiorespiratory
1243 frequencies. *Scientific reports*, *10*(1), 21559. https://doi.org/10.1038/s41598-020-77984-1
1244 119. Vaccaro, A., Tauffenberger, A., Aggad, D., Rouleau, G., Drapeau, P., and Parker, J. A.
1245 (2012). Mutant TDP-43 and FUS cause age-dependent paralysis and neurodegeneration in
1246 C. elegans. *PloS one*, *7*(2), e31321. https://doi.org/10.1371/journal.pone.0031321
1247 120. van Ham, T. J., Thijssen, K. L., Breitling, R., Hofstra, R. M., Plasterk, R. H., and Nollen,
1248 E. A. (2008). C. elegans model identifies genetic modifiers of alpha-synuclein inclusion
1249 formation during aging. *PLoS genetics*, *4*(3), e1000027.
1250 https://doi.org/10.1371/journal.pgen.1000027

121. Vidal-Gadea, A., Topper, S., Young, L., Crisp, A., Kressin, L., Elbel, E., Maples, T., Brauner, M., Erbguth, K., Axelrod, A., Gottschalk, A., Siegel, D., and Pierce-Shimomura, J. T. (2011). Caenorhabditis elegans selects distinct crawling and swimming gaits via dopamine and serotonin. *Proceedings of the National Academy of Sciences of the United States of America*, *108*(42), 17504–17509. https://doi.org/10.1073/pnas.1108673108

122. Vogel, J. W., Iturria-Medina, Y., Strandberg, O. T., Smith, R., Levitis, E., Evans, A. C., Hansson, O., Alzheimer's Disease Neuroimaging Initiative, and Swedish BioFinder Study (2020). Spread of pathological tau proteins through communicating neurons in human Alzheimer's disease. *Nature communications*, *11*(1), 2612. https://doi.org/10.1038/s41467-020-15701-2

123. Vogel, J. W., Iturria-Medina, Y., Strandberg, O. T., Smith, R., Levitis, E., Evans, A. C., Hansson, O., Alzheimer's Disease Neuroimaging Initiative, and Swedish BioFinder Study (2020). Spread of pathological tau proteins through communicating neurons in human Alzheimer's disease. *Nature communications*, *11*(1), 2612. https://doi.org/10.1038/s41467-020-15701-2

124. Vossel, K. A., Zhang, K., Brodbeck, J., Daub, A. C., Sharma, P., Finkbeiner, S., Cui, B., and Mucke, L. (2010). Tau reduction prevents Abeta-induced defects in axonal transport. *Science (New York, N.Y.)*, *330*(6001), 198. https://doi.org/10.1126/science.1194653

125. Way, J. C., and Chalfie, M. (1989). The mec-3 gene of Caenorhabditis elegans requires its own product for maintained expression and is expressed in three neuronal cell types. *Genes & development*, *3*(12A), 1823–1833. https://doi.org/10.1101/gad.3.12a.1823

126. Wegmann, S., Maury, E. A., Kirk, M. J., Saqran, L., Roe, A., DeVos, S. L., Nicholls, S., Fan, Z., Takeda, S., Cagsal-Getkin, O., William, C. M., Spires-Jones, T. L., Pitstick, R., Carlson, G. A., Pooler, A. M., and Hyman, B. T. (2015). Removing endogenous tau does not prevent tau propagation yet reduces its neurotoxicity. *The EMBO journal*, *34*(24), 3028–3041. https://doi.org/10.15252/embj.201592748

127. White, J. G., Southgate, E., Thomson, J. N., and Brenner, S. (1986). The structure of the nervous system of the nematode Caenorhabditis elegans. *Philosophical transactions of the Royal Society of London. Series B, Biological sciences*, *314*(1165), 1–340. https://doi.org/10.1098/rstb.1986.0056

128. Wu, Z., Cardona, E. A., Cohn, J. A., and Pierce, J. T. (2025). Nonapoptotic role of EGL-1 in exopher production and neuronal health in *Caenorhabditis elegans*. *Proceedings of the National Academy of Sciences of the United States of America*, *122*(2), e2407909122. https://doi.org/10.1073/pnas.2407909122

129. Wu, Z., Ghosh-Roy, A., Yanik, M. F., Zhang, J. Z., Jin, Y., and Chisholm, A. D. (2007). Caenorhabditis elegans neuronal regeneration is influenced by life stage, ephrin signaling,

1287 and synaptic branching. *Proceedings of the National Academy of Sciences of the United*
1288 *States of America*, *104*(38), 15132–15137. https://doi.org/10.1073/pnas.0707001104
1289 130. Yoshiyama, Y., Higuchi, M., Zhang, B., Huang, S. M., Iwata, N., Saido, T. C., Maeda, J.,
1290 Suhara, T., Trojanowski, J. Q., and Lee, V. M. (2007). Synapse loss and microglial activation
1291 precede tangles in a P301S tauopathy mouse model. *Neuron*, *53*(3), 337–351.
1292 https://doi.org/10.1016/j.neuron.2007.01.010
1293 131. Zhou, W., Scott, S. A., Shelton, S. B., and Crutcher, K. A. (2006). Cathepsin D-mediated
1294 proteolysis of apolipoprotein E: possible role in Alzheimer's disease. *Neuroscience*, *143*(3),
1295 689–701. https://doi.org/10.1016/j.neuroscience.2006.08.019
1296
1297 **Figure captions MAIN**
1298
1299 **Fig. 1.**
1300 **Deletion of *ptl-1* partially suppresses progressive pattern of behavioral decline induced**
1301 **by APOE4**
1302 (A left) Timeline to the adult age of onset of defective or abnormal behaviors in APOE4 strain.
1303 (A right) Endogenous *ptl-1* locus with all known isoforms and the portion deleted in the *ok621*
1304 allele as indicated below.
1305 (B-H) Results of behavioral assays, used to proxy neuronal dysfunction, are arranged by the
1306 age of onset for APOE4-induced defects. Only in the cases of gentle touch sensation and
1307 pumping behaviors (B,C) are APOE4 defects suppressed such that there are no significant
1308 differences between control and APOE4;Δ*ptl-1* groups.
1309 (B-E) D1 adult onset. (B) Subtle defect in gentle touch sensitivity which is fully suppressed by
1310 *ptl-1* deletion. N=47 for control, N=30 for Δ*ptl-1*, N=33 for APOE4, and N=35 for APOE4;Δ*ptl-1*.
1311 (C) Subtle defect in pharyngeal pumping which is fully suppressed by *ptl-1* deletion. N=94 for
1312 control, N=37 for Δ*ptl-1*, N=61 for APOE4, and N=91 for APOE4;Δ*ptl-1*. (D) Severe defect in
1313 swim-to-crawl gait transition which is partially suppressed by *ptl-1* deletion. N=164 control,
1314 N=136 for Δ*ptl-1*, N=162 for APOE4, N=165 for APOE4;Δ*ptl-1*. (E) Subtle defect in short-term
1315 locomotion which is not suppressed by *ptl-1* deletion. N=47 for control, N=38 for Δ*ptl-1*, N=44
1316 for APOE4, and N=44 for APOE4;Δ*ptl-1*.
1317 (F) D2 adult onset. Subtle defect in long-term locomotion was not suppressed by *ptl-1* deletion.
1318 N=31 control, N=32 for Δ*ptl-1*, N=28 for APOE4, and N=29 for APOE4;Δ*ptl-1*.
1319 (G,H) D3 adult onset. (G) Severe egg laying defect was partially suppressed by *ptl-1* deletion.
1320 N=196 for control, N=134 for Δ*ptl-1*, N=214 for APOE4, N=243 for APOE4;Δ*ptl-1*. (H) Subtle,
1321 abnormal increase in harsh touch sensitivity. N=25 for control, N=17 for Δ*ptl-1*, N=26 for
1322 APOE4, and N=31 for APOE4;Δ*ptl-1*.
1323 All data are represented as mean ± SEM. N is the total sample size representing all animals
1324 across replicates. Statistical comparisons were made using χ^2 tests of independence for D,G
1325 and planned tests after two-way ANOVA for B,C,E,F,G. *: $p<0.05$; **: $p<0.01$; ***: $p<0.001$.
1326
1327
1328 **Fig. 2.**
1329 **APOE4-induced behavioral decline may be the result of developmental and age-related**
1330 **defects**
1331 (A,B) Assays of gentle touch sensitivity. (A) Control worms maintained sensitivity from L4
1332 (N=18) to D1 adult (N=22) to D3 adult (N=22) age. (B) APOE4 worms showed a decrease in
1333 sensitivity from L4 (N=18) to D1 adult (N=17) and remained unchanged afterward into D3 adult
1334 (N=17) age.

1335 (C,D) Assays of pharyngeal pumping. (C) Control worms showed an expected increase in
1336 pumping behavior from L4 (N=18) to D1 adult (N=20) that remained into D3 adult (N=16) age.
1337 (D) APOE4 worms showed no difference in pumping across L4 (N=18) to D1 adult (N=17) to D3
1338 adult (N=20) ages.
1339 All data are represented as mean ± SEM. N is the total sample size. Statistical comparisons
1340 were made using planned tests after two-way ANOVA. *: p<0.05; **: p<0.01; ***: p<0.001.
1341
1342
1343 **Fig. 3**
1344 **Deletion of *ptl-1* partially suppresses APOE4-induced HSN axon dysmorphia**
1345 (A) Cartoon of the worm midbody, centered about the vulva area, depicting: the HSN proximal
1346 axon, the VC4,5 neurons, vulval musculature, and ventral nerve cord (VNC). For the proximal
1347 axon: segment i. is the initial, anteriorly projecting portion and segment ii. is the ventrally
1348 projecting portion.
1349 (B) Representative live images of normal (1,2) and abnormal (3-10) HSN proximal axons
1350 visualized with GFP. Proximal axon segments are marked by i. and ii (with exception to image
1351 2, where segment identity is less certain). The vulva area is also marked with a white arrowhead
1352 for anatomical reference. All scale bars are 20 µm.
1353 (C,D) Percentage of animals with abnormal HSN proximal axons in D1 and D3 adults. The
1354 baseline incidence of abnormal axons in control was similar between D1 and D3.
1355 (C) D1 adults. All other groups show non-significant, but slightly increased incidence of
1356 abnormal axons compared to control. N=37 for control, N=59 Δ*ptl-1*, N=51 for APOE4, N=22 for
1357 APOE4;Δ*ptl-1* (left), and N=37 for APOE4;Δ*ptl-1* (right).
1358 (D) The incidence of abnormal axons appears to correlate with defective egg laying behavior
1359 (See Fig. 1G) in D3 adults. N=101 for control, N=78 for Δ*ptl-1*, N=91 for APOE4, N=79 for
1360 APOE4;Δ*ptl-1* (left), and N=86 for APOE4;Δ*ptl-1* (right).
1361 (E,F) Quantification of HSN proximal axon lengths in D1 and D3 adults. The baseline axon
1362 length in control was similar between D1 and D3.
1363 (E) D1 adults. Axon length was similar across all groups. N=15 for control, N=13 Δ*ptl-1*, N=20
1364 for APOE4, N=6 for APOE4;Δ*ptl-1* (left), and N=10 for APOE4;Δ*ptl-1* (right).
1365 (F) D3 adults. Axon length appears to correlate with the incidence of abnormal axons shown in
1366 (C) and defective egg laying behavior (See Fig. 1G). N=79 for control, N=66 for Δ*ptl-1*, N=72 for
1367 APOE4, N=54 for APOE4;Δ*ptl-1* (left), and N=66 for APOE4;*ptl-1* (right).
1368 (G) By-day breakdown of defective egg laying as quantified cumulatively in Fig. 1G. D3 data are
1369 replotted from Fig. 1G.
1370 All data are represented as mean ± SEM. N is the total sample size representing all animals
1371 across replicates. Statistical comparisons were made using χ^2 tests of independence for C and
1372 D and planned comparisons after two-way ANOVAs for E and F. *: p<0.05; **: p<0.01; ***:
1373 p<0.001.
1374
1375
1376 **Fig. 4.**
1377 **Targeted genetic ablation, but not abolished function, of the TRNs protects HSN against**
1378 **APOE4-induced dysfunction**
1379 (A1) Egg-laying behavior across groups. Genetic ablation of the TRNs partially suppressed egg-
1380 laying defects in APOE4 animals as with the *ptl-1* deletion (See Fig. 1G). N=104 for control,
1381 N=171 for TRNs::EGL-1, N=525 for APOE4, and N=190 for APOE4;TRNs::EGL-1.
1382 (A2 top) Cartoon depicting the head and tail areas wherein the nerve ring and PLM neuron,
1383 respectively, are located.
1384 (A2 bottom) Representative live images of nerve ring (arrowhead) and PLM neuron (within
1385 dashed circle if present; marked with asterisk if absent) visualized with PTL-1::mNG in control
1386 and TRNs::EGL-1 animals. Dashed borders indicate the worm body outline. All scale bars are
1387 20 µm.

1388 (B) Egg-laying behavior across groups. In contrast to genetic ablation, abolishing TRN function
1389 did not suppress egg laying defects. N=104 for control, N=123 for *mec-4*(*lf*), N=525 for APOE4,
1390 and N=226 for APOE4;*mec-4*(*lf*).
1391 All data are represented as mean ± SEM. N is the total sample size representing all animals
1392 across replicates. All statistical comparisons were made using χ^2 tests of independence. control
1393 and APOE4 data are re-plotted in A1 and B. *: p<0.05; **: p<0.01; ***: p<0.001.
1394
1395
1396 **Fig. 5.**
1397 **Targeted depletion of PTL-1 in the TRNs protects HSN against APOE4-induced**
1398 **dysfunction**
1399 (A1) Egg-laying behavior across groups. N=104 for control, N=180 for TRNs::*ptl-1* KD, N=525
1400 for APOE4, N=171 for APOE4;TRNs::*ptl-1* KD (left), and N=108 for APOE4;TRNs::*ptl-1* KD
1401 (right).
1402 (A2) Quantification of *ptl-1* knockdown in the targeted TRNs and non-targeted VCs4,5 neurons
1403 between control and TRNs::*ptl-1* KD animals using PTL-1::mNG fluorescence intensity in the
1404 soma.
1405 (B1) Egg-laying behavior across groups. N=104 for control, N=348 for TRNs::*ptl-1* KO, N=525
1406 for APOE4, N=423 for APOE4;TRNs:: *ptl-1* KO (left), and N=519 for APOE4;TRNs:: *ptl-1* KO
1407 (right).
1408 (B2) Representative live images of nerve ring (arrowhead) and PLM neuron (within dashed
1409 circle if present; area marked with asterisk if absent) visualized with PTL-1::mNG in control and
1410 TRNs::*ptl-1* KO animals. Dashed borders indicate the worm body outline. All scale bars are 20
1411 µm.
1412 (B3) Percentage of animals with abnormal HSN proximal axons in D3 adults using independent
1413 reporter transgenics from Fig. 3. N=31 for TRNs::*ptl-1* KO and N=17 for APOE4;TRNs::*ptl-1* KO.
1414 (C) Egg-laying behavior across groups. N=104 for control, N=80 for CHEs::*ptl-1* KO, N=525 for
1415 APOE4, and N=78 for APOE4;TRNs:: *ptl-1* KO.
1416 All data are represented as mean ± SEM. N is the total sample size representing all animals
1417 across replicates. Statistical comparisons were made using χ^2 tests of independence for
1418 A1,B1,B3,C and Student's t-test for A2. Control and APOE4 data are re-plotted in A1, B1, and
1419 C. *: p<0.05; **: p<0.01; ***: p<0.001.
1420
1421

Figure1

Click here to access/download;Figure;figure1.pdf

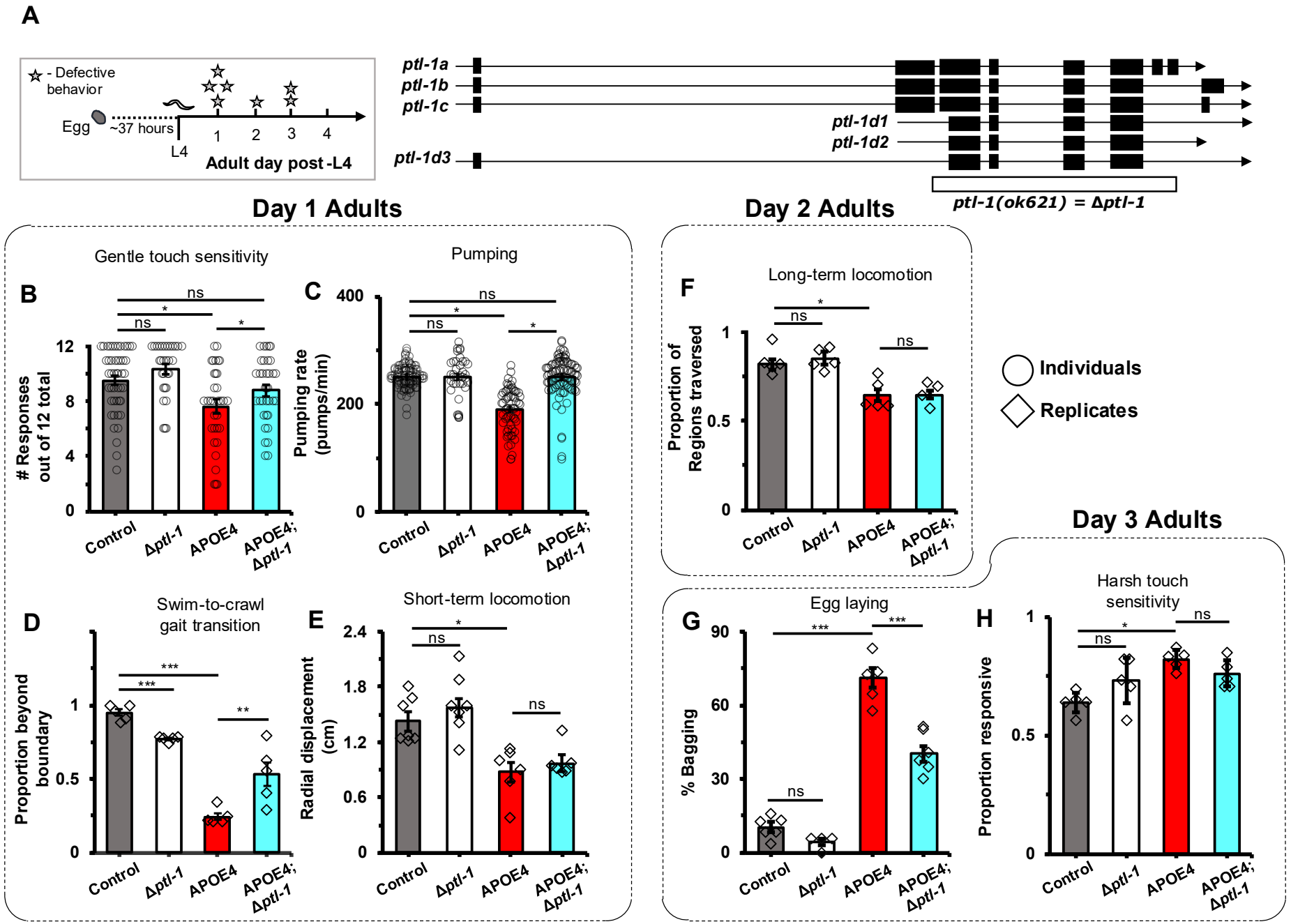

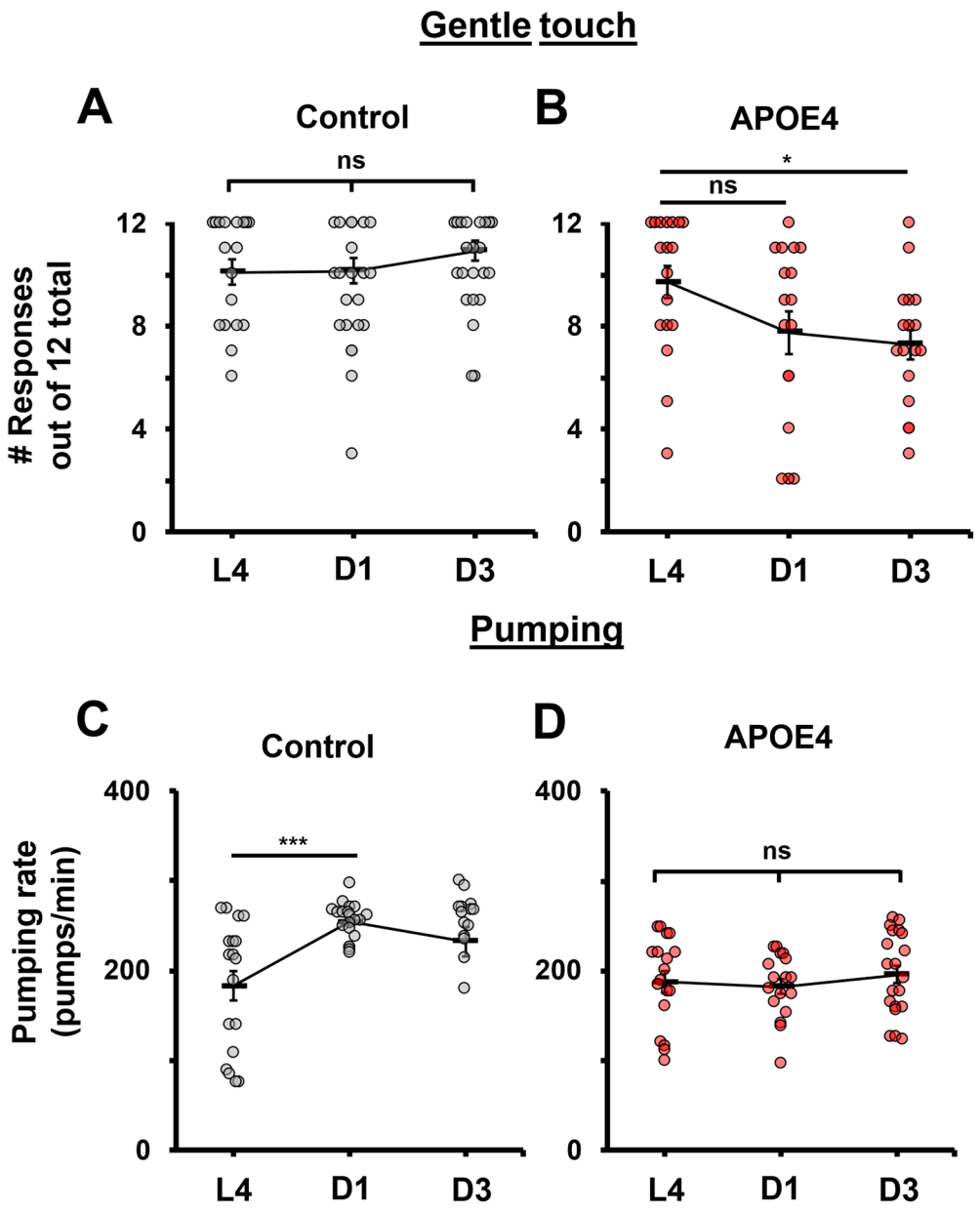
Gentle touch
A
Control
ns
B
APOE4
*
ns
Responses out of 12 total
12
8
4
0
L4
D1
D3
Pumping
C
Control
***
D
APOE4
ns
Pumping rate (pumps/min)
400
200
0
L4
D1
D3

Figure3

Click here to access/download;Figure;figure3.pdf

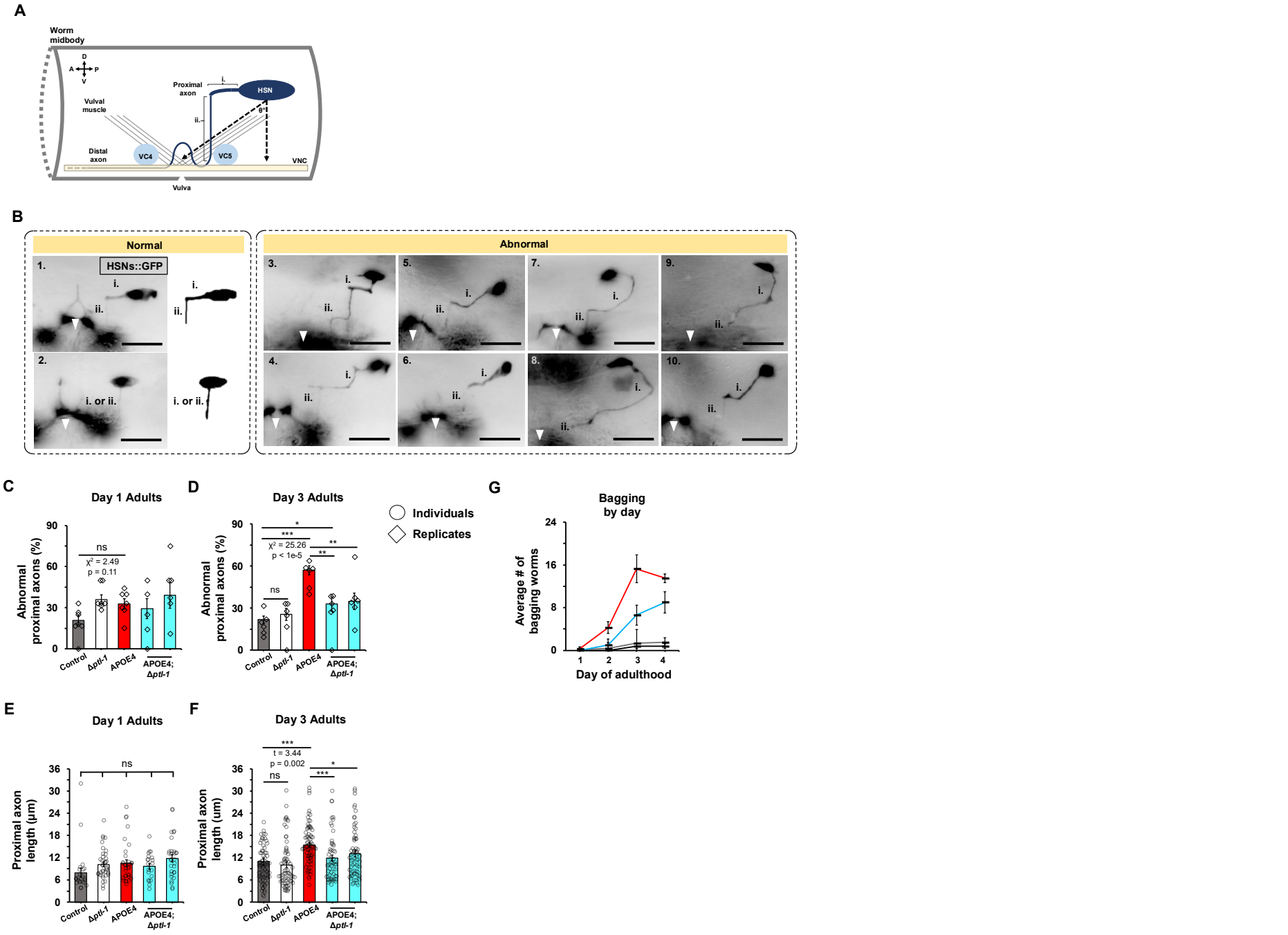

Figure4

Click here to access/download;Figure;figure4.pdf

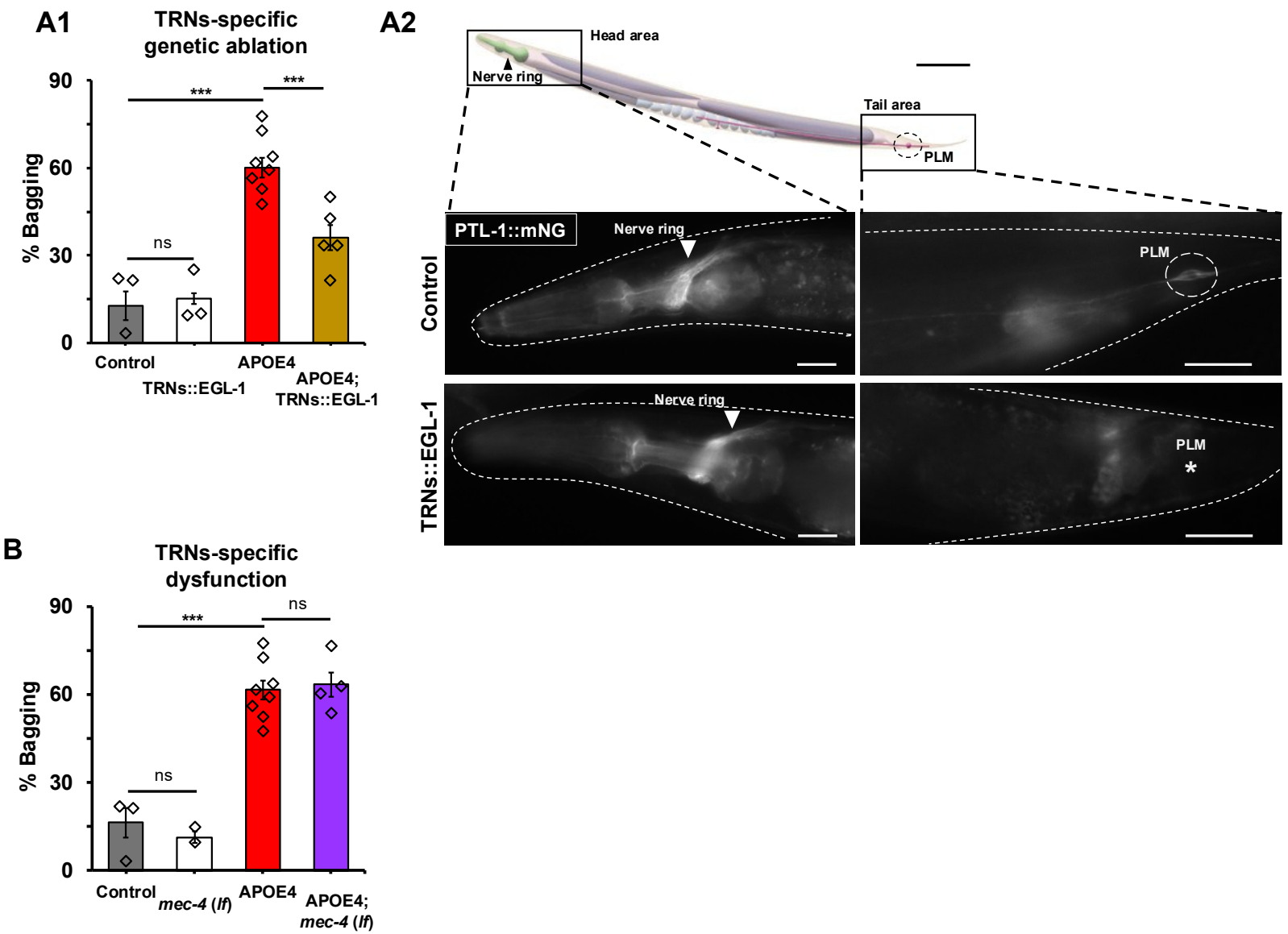

Figure5
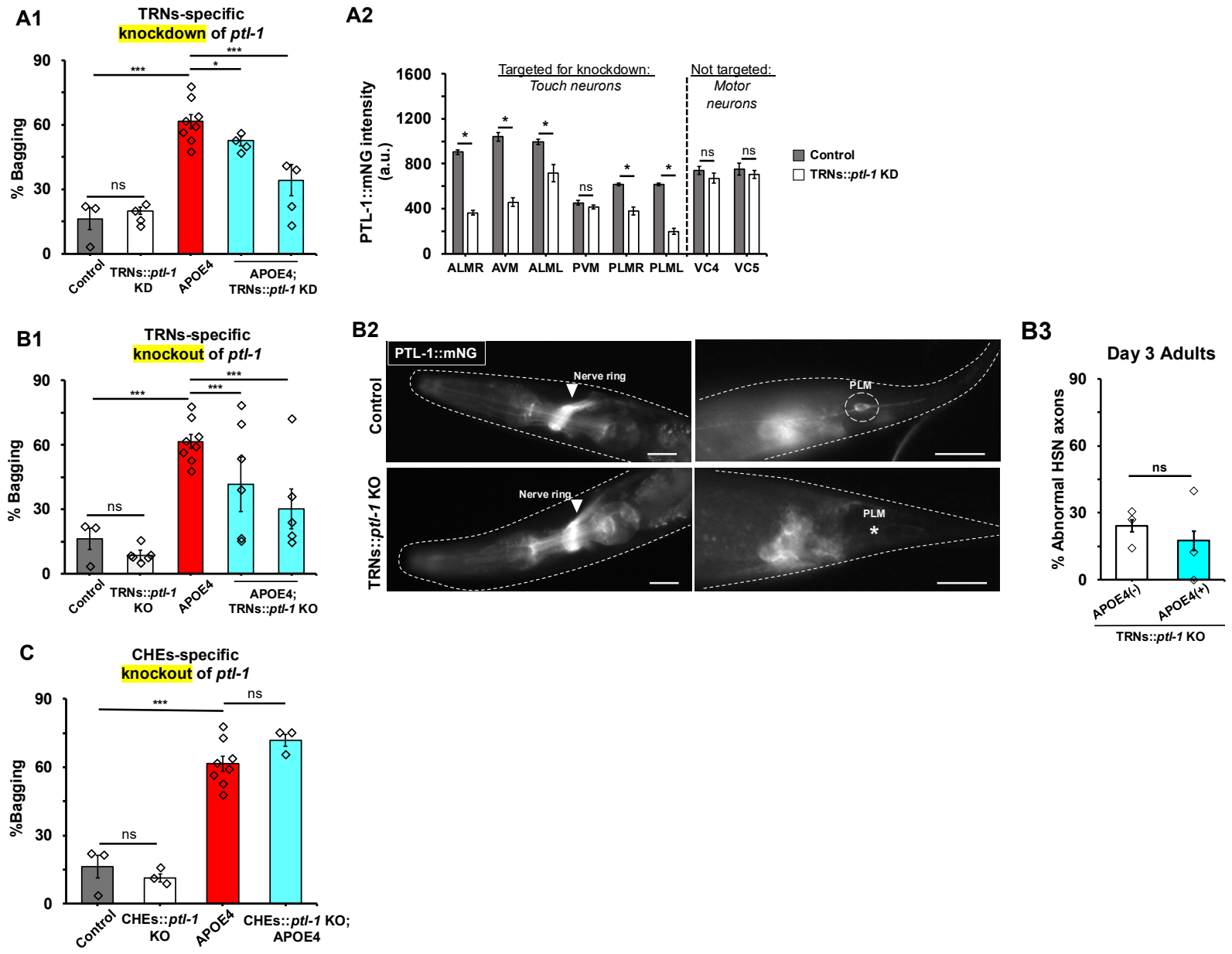
Click here to access/download;Figure;figure5.pdf